C00-1198-1216

UNIVERSITY OF ILLINOIS AT URBANA-CHAMPAIGN

THE GRADUATE COLLEGE

OCTOBER 1978

WE HEREBY RECOMMEND THAT THE THESIS BY

ROBERT JOHN LAUF

ENTITLED A STUDY OF METAL-OXYGEN SOLID SOLUTIONS

UTILIZING SOLID ELECTROLYTIC CELLS

BE ACCEPTED IN PARTIAL FULFILLMENT OF THE REQUIREMENTS FOR

THE DEGREE OF DOCTOR OF PHILOSOPHY

Director of Thesis Research

Head of Department

Committee on Final Examination†

Chairman

† Required for doctor's degree but not for master's.

O-517

DISCLAIMER

A STUDY OF METAL-OXYGEN SOLID SOLUTIONS UTILIZING SOLID ELECTROLYTIC CELLS

BY

ROBERT JOHN LAUF

B.S., University of Illinois, 1974
M.S., University of Illinois, 1974

THESIS

Submitted in partial fulfillment of the requirements
for the degree of Doctor of Philosophy in
Metallurgical Engineering in the Graduate College of the
University of Illinois at Urbana-Champaign, 1978

Urbana, Illinois

A STUDY OF METAL-OXYGEN SOLID SOLUTIONS UTILIZING SOLID ELECTROLYTIC CELLS

Robert John Lauf, Ph.D.
Department of Metallurgy and Mining Engineering
University of Illinois at Urbana-Champaign, 1978

A study has been made of the thermodynamic and kinetic behavior of oxygen in a number of Group V metals and alloys. Investigations were made with a ThO_2/Y_2O_3 electrolyte over the temperature range of 600-1150°C (873-1423°K). The activity of oxygen in three Nb-Ta alloys (nominally 25, 50, and 75 at.% Ta) was found to obey Henry's Law up to the solubility limit in each alloy. The standard entropy and enthalpy of solution of oxygen in the three Nb-Ta alloys were intermediate between those for pure niobium and pure tantalum, and varied almost linearly with Nb:Ta content.

The diffusion coefficient of oxygen was measured in niobium and vanadium, and the values were found to be in excellent agreement with literature values obtained by a variety of techniques. The diffusion coefficient of oxygen in each of several dilute substitutional niobium alloys was measured and compared to the diffusion coefficient in pure niobium. The addition of 1 to 5% substitutional solutes resulted in as much as an order-of-magnitude decrease in the oxygen diffusivity. This decrease is believed to be due to trapping of oxygen by

substitutional solute atoms. The substitutional-oxygen binding or "trap" energies (in eV) for several substitutional solutes in niobium were determined to be: Ta: 0.3 ± 0.1; V: 0.55 ± 0.05; Ti: 0.7 ± 0.1; Zr: 0.7 ± 0.05. The trap energy is rationalized as being the sum of a chemical interaction and an elastic interaction.

ACKNOWLEDGEMENT

The author wishes to thank Professor Carl Altstetter for providing continued support and guidance throughout the course of his graduate studies. He also expresses his appreciation to Dr. Gary L. Steckel for his assistance in learning the experimental technique. Thanks are also due to many friends and colleagues for their valuable assistance and helpful discussions.

The support provided by the Department of Metallurgy and Mining Engineering and the Materials Research Laboratory (U.S. Department of Energy Contract EY-76-C-02-1198 and National Science Foundation MRL Grant DMR-76-01058) is very much appreciated. The assistance of the Analytical Chemistry Group of the Materials Research Laboratory at the University of Illinois is also acknowledged.

TABLE OF CONTENTS

LIST OF TABLES

LIST OF FIGURES

1. INTRODUCTION

The refractory metals molybdenum, niobium, tantalum, tungsten, and vanadium have great potential for use as high temperature structural materials, due to their high melting points and strength at high temperatures. Because of their greater ease of fabricability, the Group V metals, niobium, tantalum, and vanadium, are of primary interest for a number of applications. Unfortunately, these materials are very reactive with oxygen and nitrogen at high temperatures, and this poses a serious restriction on their use in hostile environments.

The purpose of this research is to examine the thermodynamic and kinetic behavior of oxygen in various refractory metal alloys. The interaction between oxygen and substitutional solutes is determined from its effect on long range oxygen diffusion and/or its effect on equilibrium oxygen activity. The data are determined by the use of solid state galvanic cells. Experimental diffusion data are compared to statistical models for diffusion under the influence of randomly distributed isolated traps. These results are used to estimate the binding between the oxygen and substitutional impurity atoms.

1.1 Solid State Galvanic Cell Technique

The galvanic cell used in this study consisted of two

electrodes with different oxygen activities, separated by a solid oxide electrolyte. At high temperatures, this electrolyte conducts oxygen ions, which diffuse through it in the direction of decreasing oxygen chemical potential. At open circuit, providing the oxide does not conduct electrons, a negative charge layer builds up on the side of lower oxygen activity. Eventually, the electric potential associated with this charge layer just balances the chemical potential difference. A state of dynamic equilibrium is achieved, and the cell EMF becomes constant with time. This EMF is related to the difference in free energy of oxygen, ΔG, between the two electrodes, by the Nernst equation,

$$\Delta G = -nFE \qquad (1)$$

where n is the ionic charge (n=2 for oxygen), E is the cell EMF, and F is the Faraday constant.

In practice, one electrode is used as a reference and has a known oxygen chemical potential. The measured EMF therefore allows the determination of the unknown oxygen chemical potential of the other electrode. The assumption is made that there is only one reversible cell reaction, and that there are no reactions with the cell atmosphere or between the electrodes and electrolyte. In addition, it is assumed that all charge transport in the electrolyte is due to oxygen ion migration.

Kiukkola and Wagner (1,2) demonstrated the use of solid oxide electrolytes for the determination of standard free energies of formation of several metal oxides. Many studies have been undertaken since then for the purpose of developing

better oxide electrolytes and characterizing their properties. This work is reviewed by Etsell and Flengas (3).

The suitability of a particular electrolyte for use with a given metal/oxygen system is determined mainly by two criteria, namely, the ionic conductivity and the ionic transference number. In general, these are both dependent on temperature and oxygen partial pressure. For the electrolyte to be useful, the ionic conductivity must be great enough for equilibrium to be attained in a reasonable amount of time, and the ionic transference number must be greater than 0.99.

For use with the Group V metals, the thoria-based electrolytes are the most suitable. This is due to their thermodynamic stability and purely ionic conductance at the relatively low oxygen partial pressures encountered in these systems. The electrolyte used in this study was a solid solution of 92 mole % ThO_2 and 8 mole % Y_2O_3, and had the fluorite structure. This composition has an anion vacancy concentration of 3.75 % (3). This results in a high anion mobility relative to cation and electron mobilities. The relation between total conductivity and oxygen pressure at 1000°C is shown in Figure 1 (4-8). At this temperature the electrolyte exhibits p-type conduction at oxygen pressures greater than 10^{-5} atm (1.01 Pa) (4) and n-type conduction at oxygen pressures less than 10^{-30} atm (1.01×10^{-25} Pa) (5). Between these two extremes, the conductivity is constant and is almost entirely due to anion mobility. The range of oxygen pressures found in this investigation is indicated in the figure, and it is seen to be within the range of ionic conduction.

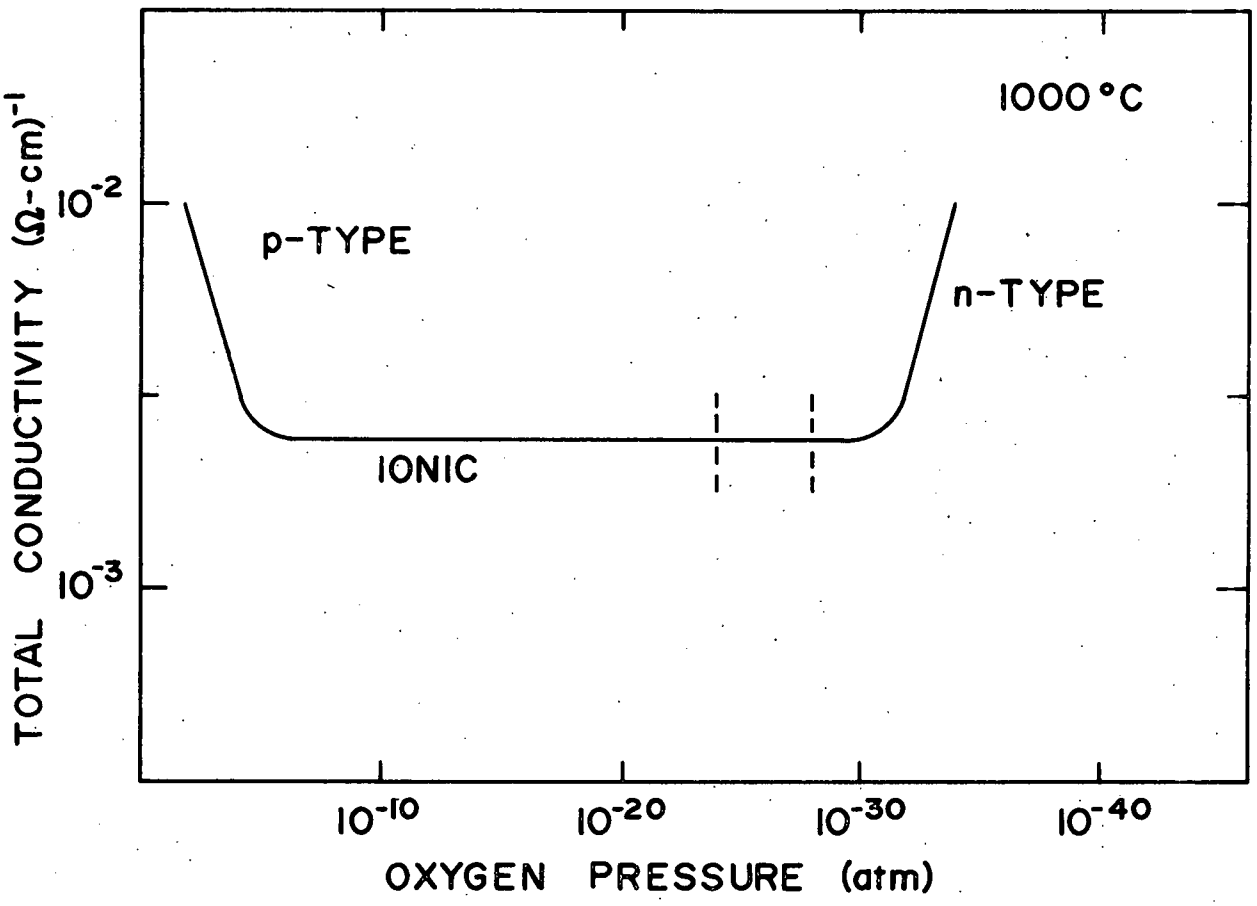

Figure 1: Logarithm of total conductivity versus logarithm of oxygen partial pressure for ThO_2/Y_2O_3 electrolyte at 1000°C. The dashed lines indicate the range of oxygen partial pressures found in this study.

1.2 Thermodynamics of the Niobium-Tantalum-Oxygen System

The terminal solubility and related thermodynamic data for oxygen in pure niobium and in pure tantalum have been reported by a number of workers. Reviews by Fromm (9) and Fromm and Jehn (10) have also been published.

However, the early results for both the niobium-oxygen system (11-15) and the tantalum-oxygen system (16-25) show some disagreement, particularly at the lower temperatures and compositions. Recently, data for the niobium-oxygen system (26) and the tantalum-oxygen system (27) have been determined using solid electrolytic cells. In these latter studies, it was found that oxygen obeys Henry's Law in pure niobium and in pure tantalum up to the solubility limit in each. The standard enthalpy and entropy of formation of a 1%* solid solution of oxygen in niobium are given as -91370 cal/mole (-382.3 kJ/mole) and -13.3 cal/mole-^{o}K (-55.6 J/mole-^{o}K) respectively (26). The standard enthalpy and entropy of solution for oxygen in tantalum are given as -92679 cal/mole (-387.8 kJ/mole) and -14.7 cal/mole-^{o}K (-61.5 J/mole-^{o}K) respectively (27).

Since niobium and tantalum form a continuous isomorphous series (28) it might be expected that niobium-tantalum alloys would have chemical properties intermediate between those of the two pure elements. One phase of the present study was undertaken to examine this area more fully.

1.3 Diffusion of Interstitial Solutes in Refractory Metals

Since the structural properties of refractory metals are

---

* All percentages are given in atomic percent.

degraded by the presence of dissolved oxygen or internal oxides, it is important to know the rate at which oxygen will diffuse through these metals at high temperatures. At the same time, an examination of the long range diffusion of oxygen in a dilute substitutional alloy can yield more fundamental information on the interaction between an oxygen atom and a single substitutional atom. This latter aspect will be dealt with in detail in the next section.

The diffusion of oxygen in pure niobium has been measured by many workers, using a variety of techniques. This topic has very recently been reviewed by Boratto and Reed-Hill (29). In that work, a least-squares analysis of all the reported data points resulted in the following: Q= 26170 cal/mole (109.5 kJ/mole) and D_o=5.3 X 10^{-3}cm^2/sec. Diffusion was governed by a simple Arrhenius relation, but the data for temperatures above about 500°C (773°K) showed a rather wide scatter.

Data for the diffusion of oxygen in vanadium has also been reviewed by Boratto and Reed-Hill (30). This system showed simple Arrhenius behavior with D_o=2.661 X 10^{-2}cm^2/sec and Q= 29805 cal/mole (124.7 kJ/mole). However, the data consist of many measurements at temperatures less than approximately 200°C (473°K), and three data points at temperatures of 1650°C (1923°K) and above, with nothing in between these two extremes. By the nature of the least-squares analysis, these three high-temperature points are given somewhat more weight than they might otherwise deserve.

Thus, because of the scatter in the oxygen-niobium diffusion data, and the pronounced lack of oxygen-vanadium data in the temperature range of this study (500-1100°C), these two systems were chosen for preliminary diffusion measurements. This also served to establish the accuracy, reliability, and applicability of the EMF-method to these systems.

Many studies have been reported on the diffusion of oxygen in substitutional alloys (31-41).

Early work by Bunn and coworkers (31) on niobium-zirconium alloys indicated the appearance of an extraordinary internal friction peak that was attributed to O-Zr clustering. However, it was not possible for these investigators to determine the s-i binding energy. Miner et al. (32) analyzed internal friction data and report activation energies for five separate Snoek relaxations in Nb-1% Zr. These correspond to the "normal" oxygen and nitrogen relaxations as well as to relaxations involving O-Zr, O-Zr-O, and N-Zr clusters.

Wert (33) reported that the binding enthalpy of the O-Zr pair in niobium "must be several electron volts." This conclusion was based on the analysis of internal friction peaks. On the other hand, Perkins and Padgett (34) measured the diffusivity of oxygen in three dilute Nb-Zr alloys. While reporting a very strong decrease in the diffusion coefficient due to the addition of approximately 1% Zr, these authors concluded that the binding enthalpy is approximately zero, and the binding entropy is $-3.26k_B$ for the O-Zr pair.

Sagues and Gibala (35) studied s-i interactions in Ta-Re-N

and Ta-Re-O alloys. The binding enthalpy of the N-Re cluster was reported to be 0.14 eV, and that of the N-Re-N cluster was given as 0.20 eV. These workers reported a wide spectrum of possible O-Re clusters which makes a quantitative determination of their binding enthalpies impossible. But, it was suggested that the O-Re binding enthalpy is probably larger than that of the N-Re pair.

Mosher and coworkers (36) report binding enthalpies of 0.31 eV for N-Zr clusters in niobium, and 0.46 eV for Zr-N-Zr clusters.

McLellan and Farraro (37) have developed a first-order statistical model for iron-based ternary solutions containing oxygen, carbon, or nitrogen, together with a substitutional solute. It was found that when there is no "misfit energy" the energetics of trapping are dictated by electronegativity differences between iron and the substitutional species.

Mondino and Seeger (38) reviewed the evidence for interactions between vacancies and interstitial solute atoms. They concluded that monovacancies can act as traps for carbon and nitrogen diffusing in iron, and probably also for oxygen and nitrogen in the Group Va metals.

There have been several attempts to classify the modes of interaction between substitutional and interstitial solute atoms. Hassen and Arsenault (39) developed a classification system based on chemical affinities. Szkopiak and Smith (40) investigated Nb-X-O and Nb-X-N systems, where X is some substitutional solute.

They analyzed the results in terms of chemical affinities, size factor, modulus factor, and first ionization potential.

Shikama and coworkers (41) investigated s-i interactions in vanadium, and developed a classification system that is similar to the previous two systems (39,40). In a qualitative way, the interaction (attractive or repulsive) is related to the ratio of the heats of formation of the oxides of the substitutional species and the matrix. For example, the heat of formation of aluminum oxide is 133 kcal/mole of oxygen, while that of vanadium oxide is about 100 kcal/mole of oxygen. Thus, since this ratio of 1.33 is greater than unity, it is predicted that aluminum atoms will attract oxygen in vanadium. This is in agreement with observation.

The effect of trapping on the solubility of nitrogen in iron was examined by Dijkstra and Sladek (42). These workers concluded that small additions of manganese increase the nitrogen solubility, according to the following equation:

$$C=C_{Fe}\left[1+2C_{Mn}\exp(\Delta G/RT)\right] \qquad (2)$$

where C is the total nitrogen solubility, C_{Fe} is the nitrogen solubility in a pure Fe-N alloy, C_{Mn} is the manganese content, and ΔG is the difference in free energy of nitrogen between the normal and preferred sites. This trap energy, ΔG, was suggested to be 2800 cal/mole (11.7kJ/mole), or 0.12 eV (42).

Enrietto (43) reported that the addition of manganese to iron, in concentrations of up to 0.75%, had little influence on

the nitrogen solubility above 250°C, while as little as 0.15% Mn inhibited the precipitation of iron nitrides, especially Fe_4N. This effect was not attributed to trapping, since only about 11-12% of the nitrogen atoms were calculated to be trapped. If the precipitation kinetics were limited by nitrogen mobility, such small trapping could not account for the large decrease in nitride precipitation rate (about a factor of 10). Enrietto concluded that this decrease was due instead to an inhibition of nitride nucleation.

The question of whether interstitial atoms normally occupy octahedral or tetrahedral sites in a BCC crystal has not been conclusively answered. This is an important issue, since the model (44) that is normally used to relate internal friction data to an actual diffusion coefficient makes the assumption that interstitial jumps involve only octahedral sites.

McLellan and coworkers (45) developed a model to explain the high temperature anomaly in the diffusivity of carbon in ferrite. This model takes into account the possibility of both octahedral and tetrahedral occupancy. This model was refined by Condit and Beshers (46) who concluded that, at least for carbon in ferrite, the existence of multiple diffusion paths (i.e., o-t, o-o, and t-t) is possible.

A recent paper by Beshers (47) reviews the experiments that are being undertaken to determine which systems involve primarily octahedral site occupancy and which involve tetrahedral site occupancy.

1.4 Theoretical Models for Diffusion with Trapping

The theoretical analysis of interstitial diffusion under the influence of "trapping" defects (e.g., solute atoms, dislocations, etc.) may be approached from a number of viewpoints (34, 48-51). Two of these models (34, 49) will be presented here in detail. Discussion of the others will be presented in Section 4.2.

McNabb and Foster (48) developed a model to explain the anomalous diffusivity and solubility behavior of hydrogen in steel. The results are applicable to other interstitial solutes as well. The mathematical treatment consisted of modifying Fick's Laws, making the assumption that the diffusing species periodically encounters certain sites where it is delayed temporarily. Approximate and exact solutions to the resulting differential equations were obtained for various simple geometrical shapes. A major shortcoming of the model is that it involves several adjustable parameters that are difficult to determine experimentally.

Caskey and Pillinger (51) obtained approximate solutions to the nonlinear partial differential equations derived by McNabb and Foster (48). The finite difference method was applied to these equations, with boundary conditions appropriate to interstitial permeation and evolution in a plane. This technique will be discussed more fully in Section 2.7.

1.4.1 Oriani Model

Oriani (49) developed a simplified model, based on the

work of McNabb and Foster. This model is less general, and applicable only to certain ranges of composition. Its major advantage is the use of a single parameter to characterize the trapping statistics. This parameter is readily related to experimental measurements.

In this model, the crystal is assumed to contain two kinds of interstitial sites for occupancy by the oxygen. Most sites are normal sites characterized by the standard enthalpy of solution, ΔH^{o}, with respect to gaseous oxygen. A smaller number of sites, called "extraordinary" sites or traps, provide a more energetically favored environment for the oxygen atom:

$$[O]_n \longrightarrow [O]_x \qquad \Delta E_x \qquad (3)$$

Providing the trap density is small, it can be assumed that the traps do not appreciably reduce the cross-section for normal diffusion. Then, Fick's Law can be written for the flux, J, in terms of the occupied normal sites only:

$$J=-D_n\frac{dc_n}{dx} \qquad (4)$$

where D_n is the normal diffusivity and c_n is the oxygen concentration on normal interstitial sites. But, in most experiments the important parameter is the relation between the observed flux and the gradient of total concentration, c_T, which is the sum of c_n and the concentration in extraordinary sites, c_x:

$$J=-D\frac{dc_T}{dx} \qquad (5)$$

This quantity D may be viewed as an apparent or phenomenological diffusivity, and its relation to D_n may be derived by assuming that local equilibrium exists between the trapped and untrapped populations, both in the static case ($J=0$) and during diffusion.

The equilibrium between the two populations, each occupying a fraction θ_i of the available sites, can be described by an equilibrium constant, $K=a_x/a_n$, where a_x and a_n are the oxygen activities on the extraordinary and normal sites, respectively. The activities can be expressed as $a_i=\theta_i/(1-\theta_i)$ where the reference state is $a_i=\theta_i$ when $\theta_i \longrightarrow 0$. Also, since low concentrations are the only ones being considered, $\theta_n \ll 1$ so that the local equilibrium constant for reaction (3) may be written as:

$$K=\frac{1}{\theta_n}\left[\frac{\theta_x}{1-\theta_x}\right] \tag{6}$$

Thus, the relation between the apparent diffusivity, D, and the normal diffusivity, D_n, is given by:

$$D=D_n\left[\frac{c_n}{c_n+c_x(1-\theta_x)}\right] \tag{7}$$

For the case where $\theta_x \ll 1$, $D=D_n(c_n/c_T)$.

Finally, the equilibrium constant can be expressed as:

$$K=\exp(-\Delta E_x/kT) \tag{8}$$

To apply the foregoing to experimental data, the following approach may be used. Consider N atoms of niobium with some

fraction X_s (less than about 4%) of a substitutional species such as vanadium or zirconium. There will be 3N normal interstitial sites, and $3N \cdot 2X_s$ trapping sites. (The factor of two arises from geometrical considerations.) Providing θ_x and θ_n are $\ll 1$, the following simplification applies:

$$K=\frac{\theta_x}{\theta_n}$$

And,
$$D=D_n\left[\frac{c_n}{c_n+c_x}\right]$$

where
$$c_n=N_n\theta_n=3N\theta_n$$

and
$$c_x=N_x\theta_x=3N(2X_s)K\theta_n$$

Thus,
$$D=D_n\left[\frac{3N\theta_n}{3N\theta_n+3N\theta_n(2KX_s)}\right]$$

or,
$$D=D_n\left[\frac{1}{1+2KX_s}\right] \qquad (9)$$

In this way, knowing D_n for oxygen in pure niobium and measuring D for oxygen in some alloy of X_s substitutional content, the value of K is obtained at a particular temperature or temperatures. From this, the trap depth, ΔE_x, comes out directly.

Alternatively, knowing D_n as a function of temperature and assuming some values for ΔE_x and alloy content X_s, it is easy to calculate expected values for the phenomenological diffusivity, D. A family of such curves can be generated for constant X_s by varying ΔE_x. The one that best fits the data for a given alloy provides the "best value" for the trap energy, ΔE_x. The assump-

tion of small θ_x and small θ_n can always be checked a posteriori to make certain that the simplification is valid for the particular system under investigation.

1.4.2 Perkins and Padgett Model

This model was developed to explain the effect of zirconium additions ($\frac{1}{2}$ to 1% Zr) on the diffusion of oxygen in niobium (34).

The Gibbs free energy of binding, G_b, is defined as the decrease in free energy of the crystal as an oxygen atom is moved from infinite separation to a nearest-neighbor octahedral site adjacent to a zirconium atom. The binding enthalpy and entropy are similarly defined so that

$$G_b = H_b - TS_b \tag{10}$$

In practice, an oxygen atom beyond the next-nearest-neighbor position can be treated as being at infinite separation.

A random-walk analysis results in the following relation for the average squared migration distance $\bar{R}^2$:

$$\bar{R}^2 = 6D_n t \tag{11}$$

where D_n is the normal diffusion coefficient and t is the diffusion time. The effective diffusivity, D, is then governed by the average time that an interstitial atom spends trapped and the time that it spends freely diffusing.

The jump frequency of an oxygen atom between normal octahedral sites is given by:

$$w_1 = \nu \exp(-\Delta G_m / kT) \tag{12}$$

where ν is the vibrational frequency of the oxygen atom and ΔG_m is the free energy of migration, given by:

$$\Delta G_m = \Delta H_m - T\Delta S_m \tag{13}$$

The migration enthalpy, ΔH_m, is the same as the "activation energy", Q.

The jump frequency for an oxygen atom from a NNN site to a NN site adjacent to a zirconium atom is:

$$w_2 = \nu \exp\left[-(\Delta G_m - \tfrac{1}{2}G_b)/kT\right] \tag{14}$$

and for the reverse jump,

$$w_3 = \nu \exp\left[-(\Delta G_m + \tfrac{1}{2}G_b)/kT\right] \tag{15}$$

The average time that an oxygen atom is mobile, t_m, after leaving one trap and before entering another, is the reciprocal of the trapping frequency, ν_T, given by:

$$\nu_T = 4w_1 \cdot {}^4P_{NNN} \cdot P_{NN} \tag{16}$$

where ${}^4P_{NNN}$ is the probability of the oxygen entering a NNN site by random jumps, and P_{NN} is the probability that a NNN oxygen atom will jump into a NN site. P_{NNN} is the fraction of zirconium-NNN sites in the crystal,

$$P_{NNN} = 4X_s/(1-2X_s) \tag{17}$$

P_{NN} is given by:

$$P_{NN} = 2w_2/(2w_1+2w_2) \tag{18}$$

Combining equations (12) and (16-18) the following expression

is obtained for the trapping frequency:

$$\nu_T = 16\left[\frac{4X_s}{1-2X_s}\right]\left[\frac{w_2}{w_1+w_2}\right]\nu\exp\left[\frac{\Delta G_m}{kT}\right] \tag{19}$$

The average time that an oxygen atom spends trapped, t_{im}, is the reciprocal of the escape frequency, ν_E, from the trap:

$$\nu_E = 4w_3 \cdot P_{3NN} \tag{20}$$

where P_{3NN} is the probability that an atom on a NNN site will jump to a site further from the trapping atom, and

$$P_{3NN} = 2w_1/(2w_1+2w_2) \tag{21}$$

Combining equations (15) and (20-21) yields the following:

$$\nu_E = 4\left[\frac{w_1}{w_1+w_2}\right]\nu\exp\left[-(\Delta G_m+\tfrac{1}{2}G_b)/kT\right] \tag{22}$$

The effective diffusivity, D, can be related to the normal diffusivity by again considering the random-walk, equation (11):

$$\bar{R}^2 = 6D_n t_m \tag{23a}$$

$$= 6D(t_m+t_{im}) \tag{23b}$$

Rearranging,

$$\frac{D_n}{D}-1 = \frac{t_{im}}{t_m} \tag{24a}$$

$$= \frac{\nu_T}{\nu_E} \tag{24b}$$

Substituting the expressions for ν_T and ν_E into equation (24b) yields the final result:

$$\frac{D_n}{D} - 1 = 4\left[\frac{4X_s}{1-2X_s}\right] \cdot \exp(-S_b/k)\exp(H_b/kT) \qquad (25)$$

This expression, combined with experimental values of D, enables one to obtain values for the binding enthalpy and entropy of the O-Zr pair.

2. EXPERIMENTAL PROCEDURE

2.1 Preparation of Electrolytes

The electrolytes used in this study were of two types. Those used in the thermodynamic study of niobium-tantalum-oxygen solutions were made by G. L. Steckel at the Materials Research Laboratory at the University of Illinois. The details of their manufacture are presented elsewhere (52). These were prepared for use by polishing through $\frac{1}{4}\mu$ diamond paste.

The electrolytes used in the kinetic measurements were of a commercial type, supplied by Zirconium Corporation of America. As received, this material was approximately 3 mm thick. In order to decrease the response time of the cell, the electrolyte was sliced with a diamond saw to a final thickness of 1 mm. This thin slice was then polished through $\frac{1}{4}\mu$ diamond paste in the same manner as before.

2.2 Preparation of Alloys

The niobium-tantalum alloys were supplied in strip form by Prof. David Peterson (Iowa State University). The pure niobium was purchased in rod form from Wah Chang Albany Corp., and the pure vanadium was donated by the U.S. Bureau of Mines in the form of cast bars of approximately 11.5 x 6.5 x 1.2 cm. The titanium and zirconium were polycrystalline bars produced by the iodide process. The chemical analyses of all starting materials are given in Table I.

The alloys were prepared by arc-melting in a furnace having

TABLE I

Analyses of Starting Materials (Atomic ppm)

	Nb	V	Ti	Zr
Na	<20	---	interference	interference
Al	50-200*	---	20	90
Si	200	<27	3	interference
K	<20	---	---	3
Ca	<20	---	0.2	10
Ti	---	---	bal	10000
V	30	bal	2	0.3
Cr	30	---	10	200
Fe	30	---	10	800
Ni	---	5	---	70
Cu	50	<8	3	20
Zr	400	---	12	bal
Nb	bal	---	≤0.5	1
Mo	40	---	5	---
Hf	12	---	20	200
Ta	100	---	---	interference
W	30	---	---	interference
			Sn	10000

Analyses of Nb, Ti, and Zr were done by mass spectrographic analysis at the Materials Research Laboratory, University of Illinois.

The analysis given for V is the lot analysis given by the Bureau of Mines. All other impurities are below the detection limits of emission spectrography.

* Aluminum seemed to be inhomogeneous.

a copper crucible and an argon atmosphere. A zirconium pellet was melted first in a separate part of the crucible to act as a getter for residual oxygen and other impurities in the atmosphere. The alloy ingot was turned and melted four times to insure homogeneity.

The resulting ingots were typically 10 mm in diameter and 25 - 30 mm long. The ingots were then swaged to 3.1 mm diameter and cold-rolled into strips 0.6 mm thick. The materials were quite ductile throughout the operation and required no intermediate annealing. Sections of each strip were analyzed by electron microprobe and spectrophotometric techniques. The analyses of all the alloys used are shown in Table II.

2.3 Electrode Preparation

The samples were prepared by doping the metal strips with measured amounts of oxygen in a high-vacuum Sieverts' apparatus. This apparatus is described in detail elsewhere (53). The strips were annealed for approximately 12 hours at 1100-1300°C (1373-1573°K) at pressures in the low 10^{-7} torr (10^{-5} Pa) range. The pumps were then closed and the oxygen allowed to leak in slowly, to prevent the formation of an oxide layer on the surface of the strip. The strips were annealed for ½ hour with the pumps closed, to insure that all of the oxygen had been absorbed. The pumps were then opened to the chamber, and an homogenization anneal was carried out in vacuum with the specimens held at approximately 1300°C (1573°K) for 3 to 4 hours. The specimens were then slowly cooled to about 1000°C and then radiation cooled to room temperature.

TABLE II

Analyses of Niobium Alloys

Major constituents (atomic %)							
Nb	73.7	48.0	22.6	Nb	98.57	97.3	94.9
Ta	26.3	52.0	77.4	V	1.43	2.7	5.1
Impurities (atomic ppm)							
Na	<1	<1	<1		---	---	<1
Mg	0.6	0.3	0.5		0.2	---	<0.1
Al	1	1	0.4		5	3	6
Si	40	20	6		9	≤5	6
K	<0.5	<0.5	<0.5		---	---	<0.5
Ca	0.9	1	0.9		0.1	---	0.3
Ti	0.3	0.6	0.2		2	---	0.1
Cr	6	3	0.6		1	≤6	5
Mn	0.03	0.2	0.03		2	---	0.4
Fe	40	9	2		3	≤2	2
Co	0.04	0.03	0.03		0.07	---	0.03
Ni	8	3	2		0.09	---	0.2
Cu	1	0.6	0.2		10	4	4
Zn	0.2	---	---		---	---	<0.06
Zr	1	30	4		0.5	---	0.8
Mo	0.6	2	2		6	4	1
Hf	---	---	---		0.05	---	<0.08
Ta	major	major	major		30	≤40	20
W	20	40	50		2	5	4

Concentrations of major components were determined at the Materials Research Laboratory, University of Illinois, by titrimetric and spectrophotometric analysis.

Impurity levels were determined at the Materials Research Laboratory, University of Illinois, by mass spectrographic analysis

Carbon and nitrogen levels for alloys produced by this technique are typically 300-400 ppm or less (52).

TABLE II (Continued)

Analyses of Niobium Alloys

Major constituents (atomic %)					
Nb	99.1	Nb	99.05	Nb	95.9
Ti	0.9	Zr	0.95	Ta	4.1
Impurities (atomic ppm)					
Na	**		1*		---
Mg	20		<3		---
Al	2		30		10
Si	4		50		10
K	---		---		---
Ca	0.2		3		2
Ti	major		20		≤3
Cr	0.1		10		≤2
Mn	0.2		≤0.5		---
Fe	0.8		30		≤1
Co	0.02		3		---
Ni	0.06		1		---
Cu	3		20		10
Zn	0.08		---		---
Zr	0.04		major		≤0.9
Mo	0.1		≤10		3
Hf	---		100		---
Ta	20		100		major
W	1		50		4

* Inhomogeneously distributed in sample; may be due to surface contamination.

** Interference present which prevented determination of levels of this component.

The niobium-tantalum alloys were doped with 0.2 to 3.1 % oxygen. The alloys used in the kinetic measurements were doped to 0.5 to 0.6 % oxygen. The final oxygen concentrations were analyzed by Leco Corp. using a vacuum fusion technique.

The strips were cut into segments 13 x 7 x 0.6 mm. The surfaces were ground through 4/0 emery paper. The niobium-tantalum electrodes were then attack polished through 0.05 μ alumina in a chromic acid slurry. This produced a flat shiny surface on both sides of the electrode. The samples used in the kinetic study were ground as above and then polished on a 6 μ diamond lap. This resulted in a surface that was not as shiny as those produced by attack polishing, but was slightly flatter. This enhanced the intimate contact required at the sample/zirconium interface.

The zirconium "sinks" used in the kinetic study were made from a polycrystalline bar of iodide process zirconium. A 10 mm thick slice of the bar, 20 mm in diameter, was cold-rolled to about 3 mm thick. Rectangular sections were cut from this with dimensions slightly greater than those of the samples, typically 10 x 15 x 3 mm. One face was ground and polished through 6μ diamond, and platinum leads were spot welded onto the opposite face.

2.4 Experimental Apparatus and Technique

The vacuum furnace used in this study is shown schematically in Figure 2. The electrolytic cell was supported between two high density alumina rods mounted vertically in the center of

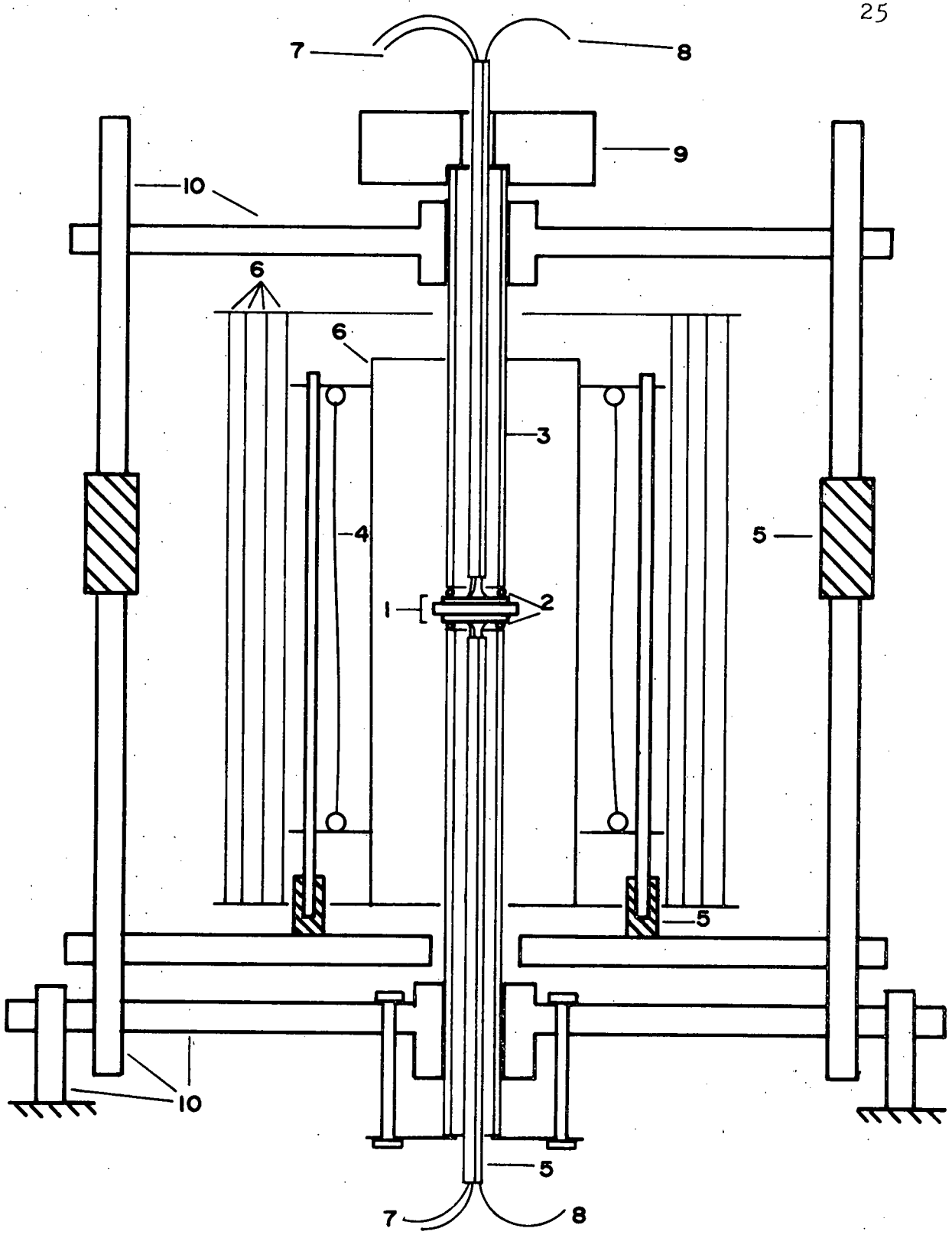

Figure 2: Schematic illustration of the experimental apparatus

1. electrolytic cell	5. ceramic insulators	9. weight
2. platinum rings	6. niobium shields	10. frame
3. Lucalox tube	7. thermocouple leads	
4. furnace element	8. EMF leads	

the furnace. A platinum ring above and below the cell helped to insure good alignment and tight contact of the cell components at high temperatures by allowing the assembly to creep into place. A stainless steel weight of 1.4 kg was placed on top of the upper support tube. This provided the stress needed to compress the platinum rings, producing the tight contact necessary for good operation of the cell. Heat was provided by a thoriated tungsten filament, operating on alternating current. The temperature was controlled by a proportional controller using the upper thermocouple. The temperature gradient between the upper and lower electrodes was typically less than $3^{o}C$.

One cylindrical niobium sheet separated the electrode compartment from the furnace element, and six concentric layers of sheet surrounded the entire assembly. These niobium sheets acted as a getter for impurities, as electrical shielding, and as thermal barriers to keep the temperature stable with time. The pressure was typically 10^{-6} to 10^{-8} torr (10^{-4} to 10^{-6} Pa).

The cell was carefully isolated electrically to insure accurate EMF measurements. The lower electrode was grounded, and the upper electrode support was isolated from the lower by alumina spacers at room temperature. The cell EMF was measured using a high impedence (10^{12} ohm) electrometer. The output of the electrometer was connected to a digital printer, which printed the date, time, upper and lower thermocouple output, pressure gage output, and cell EMF, at ten minute intervals. To save time, a double cell was used for most equilibrium EMF measurements. This is illustrated in Figure 3-(b).

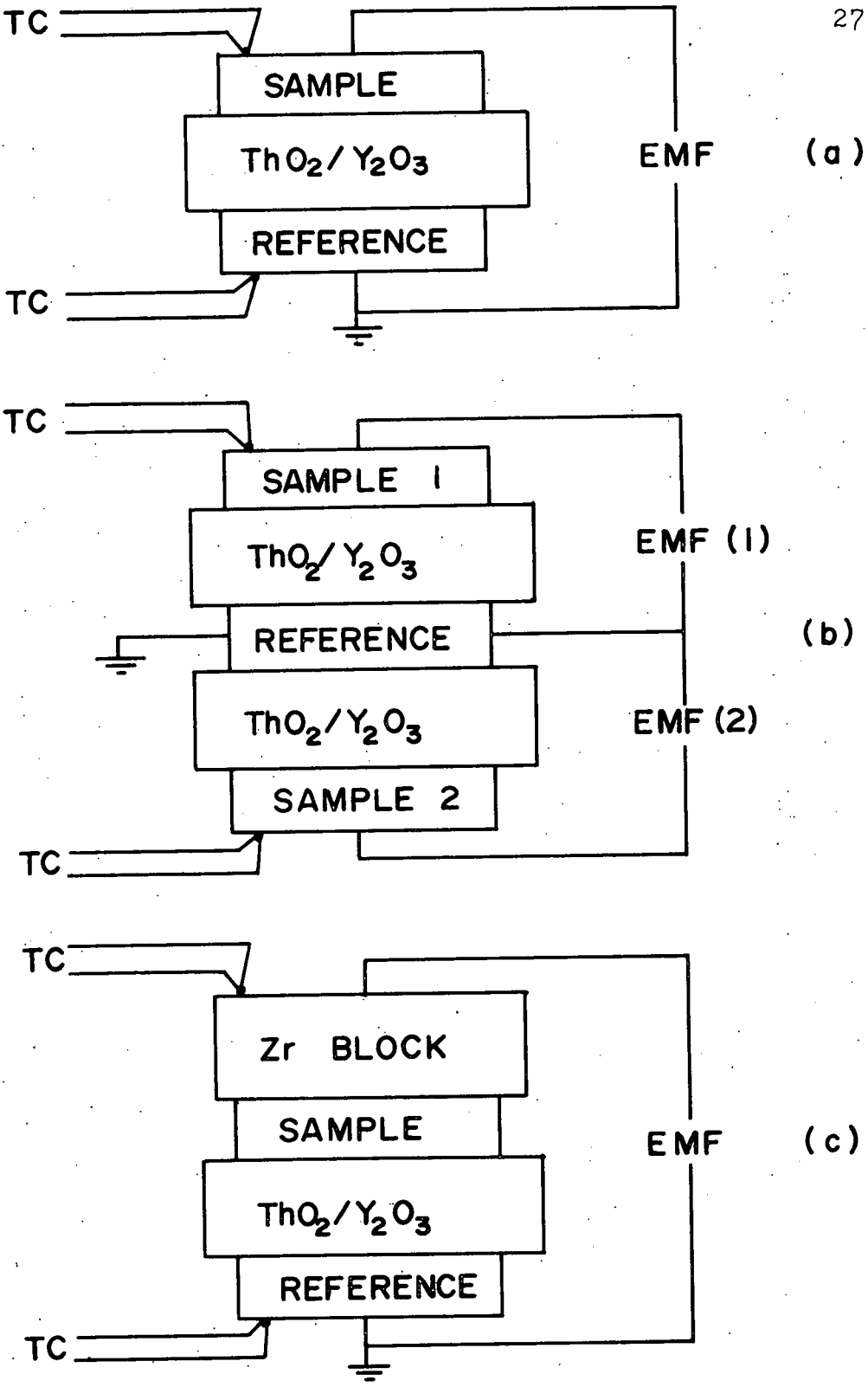

Figure 3: Cell configurations used in this study: (a) and (b), thermodynamic study of Nb-Ta-O system; (c), kinetic study.

2.4.1 Technique for Thermodynamic Study

For the study of niobium-tantalum alloys, the electrodes were placed in the cell and the leads spot-welded together. After positioning the heat shields, the system was sealed and pumped down. After baking out the chamber, the furnace was slowly heated up, maintaining vacuum. The temperature was brought to 1000°C (1273°K) in 6 to 8 hours. It was then held at this temperature until the EMF became constant with time (generally 8 to 12 hours). The EMF and actual temperature were recorded and the furnace set for a new temperature (e.g., 900°C). Equilibrium was reached at the new temperature in 2 to 4 hours and another data point was recorded. This continued down to 600°C. Then, points were taken at 650, 750, 850°C, and so on up to 1050-1100°C. The resulting plot of EMF versus temperature showed no hysteresis, and points taken at the same temperature were generally reproduceable to within 2 mV.

2.4.2 Technique for Kinetic Study

The basic arrangement of the apparatus was much the same in the kinetic study, with the following differences:

1. The reference electrode was placed on the bottom and was not disturbed for several consecutive runs. This was possible since only a single cell was used.

2. Since measurements had to be taken in a fixed time period, heating up was done at a somewhat faster rate. The furnace was held at about 300°C for $\frac{1}{2}$ hour and then brought to 1000°C in approximately one hour.

3. The EMF was recorded as a function of time. After a

sufficient time was allowed for this EMF curve to show a distinct straight-line portion with a slope that could be calculated with confidence, the temperature was changed and a new curve of EMF versus time was obtained. This is discussed more fully in Section 2.6. The cell arrangement is illustrated in Figure 3-(c).

2.5 Cell Arrangement for Nb-Ta-O Study

EMF measurements were made on the following cell:

I	Nb-Ta-O solid solution	ThO_2/Y_2O_3 electrolyte	V + 10.0 at% O $\alpha+\beta$ phases

The reaction for cell I is

$$[O]_V \longrightarrow [O]_{Nb-Ta} \qquad (26)$$

The equilibrium EMF, E, for this cell is related to the difference in Gibbs free energy of oxygen between the two-phase vanadium-oxygen alloy and the niobium-tantalum-oxygen solid solution by the Nernst equation:

$$\Delta G_1 = -nFE \qquad (1)$$

The known free energy change, ΔG_2, for oxygen gas in equilibrium with oxygen in the vanadium ($\alpha+\beta$) mixture (54) is added to ΔG_1 to obtain ΔG, the free energy change for the overall reaction

$$\tfrac{1}{2}O_2\ (g) \longrightarrow [O]_{Nb-Ta} \qquad (27)$$

Thus, cell I is used to determine the change in thermodynamic functions when molecular oxygen dissolves in niobium-tantalum alloys.

2.6 Cell Arrangement for Kinetic Study

For this phase of the research, EMF measurements were made on the following cell:

II	Zr	Alloy + O solid solution		ThO_2/Y_2O_3 electrolyte		reference electrode

The usefulness of this cell for kinetic measurements was first demonstrated by Kirchheim and coworkers (55). It was shown that the cell EMF is given by the following relation:

$$E=\frac{RT}{2F}\ln(a/a_r) \qquad (28)$$

where a is the oxygen activity at the sample/electrolyte interface, and a_r is the corresponding activity of the reference electrode.

Assuming that Henry's Law is obeyed, equation (28) can be written as:

$$E=\frac{RT}{2F}\ln(c/c_r) \qquad (29)$$

where c is the oxygen concentration.

Since the free energy of oxygen in zirconium is approximately 100 kJ/mole lower than in the niobium alloys used here, the oxygen concentration at the alloy/zirconium interface (x=0) is effectively brought to zero, or $c(0,t)=0$. Due to the low capacitance of the cell (several pico-farad) only a very negligible amount of oxygen is exchanged at the sample/electrolyte interface. Therefore, at x=L the condition is that $\frac{dc}{dx}=0$ and the initial condition is $c(x,0)=C_o$. Thus, the following solution to

Fick's second law is obtained (56):

$$c(x,t)=C_o\sum_n \sin\frac{n\pi x}{2L}\cdot\exp(-t/\tau_n) \qquad (30)$$

where $n=1,3,5,\ldots$

and $$\tau_n=\frac{1}{D}\left[\frac{2L}{n\pi}\right]^2$$

For $t>\tau_1$, $c(x,t)$ can be closely approximated by the first term in the series:

$$c(x,t)=C_o\sin\frac{\pi x}{2L}\cdot\exp\left[-\frac{\pi^2 Dt}{4L^2}\right] \qquad (31)$$

The EMF of the cell depends on the oxygen concentration at x=L, thus,

$$E(t)=\frac{RT}{2F}\ln(C_o/c_r)-\left[\frac{RT\pi^2 D}{8FL^2}\right]t \qquad (32)$$

So a plot of EMF versus time will be linear with a slope given by:

$$\frac{dE}{dt}=-\frac{RT\pi^2 D}{8FL^2} \qquad (33)$$

The diffusion coefficient is then easily calculated from equation (33). When the temperature is changed to a new value, the slope of the EMF curve changes and a new straight-line portion is formed. In practice, values of D at several temperatures may thus be obtained before electronic conduction causes deviations in the EMF. (This limitation will be discussed more fully in Section 3.2.)

2.7 Computational Technique

The mathematical modeling of diffusion with trapping was

performed on the Digital Equipment Corp. DEC 20 digital computer with a Tektronix 4010 interactive graphics terminal. Programming was done in the Fortran language. Plotting was done with the Calplot plotting subroutine, modified for interactive use. The computational treatment consisted of a modification of the technique of Caskey and Pillinger (51). This is presented in the Appendix.

3. RESULTS

3.1 Equilibrium in the Niobium-Tantalum-Oxygen System

The raw EMF data for cell I are presented in Figures 4-6 for the nominally 25, 50, and 75 % Ta alloys respectively. Straight lines were fitted to the data using a least-squares analysis.

The following equation,

$$\Delta G = -nFE = \Delta G^{o} + RT \ln \gamma X \qquad (34)$$

can be used to interpolate compositions to find E_o, the EMF for a 1 % solution. The data for different temperatures are normalized by noting that

$$\Delta G^{o} = -nFE_o \qquad (35)$$

and thus,

$$nF(E-E_o)/RT = -\ln\gamma - \ln X \qquad (36)$$

When all the data are plotted as $nF(E-E_o)/RT$ versus $\ln X$ (X = atomic percent oxygen) the points will form a straight line with a slope of -1 if Henry's Law is obeyed. By choosing the standard state to be a 1% solution, γ=1.0 for all alloys studied.

Figure 7 shows the data points for the three alloys. The solid line is a plot of Henry's Law, and it can be seen that the data points for all of the alloys are well-represented by Henry's Law. This is true for all Nb:Ta proportions and all oxygen concentrations studied, in the range of 600°C to 1100°C.

The standard free energy of solution, $\Delta G_1^{o}(T)$ can be calculated

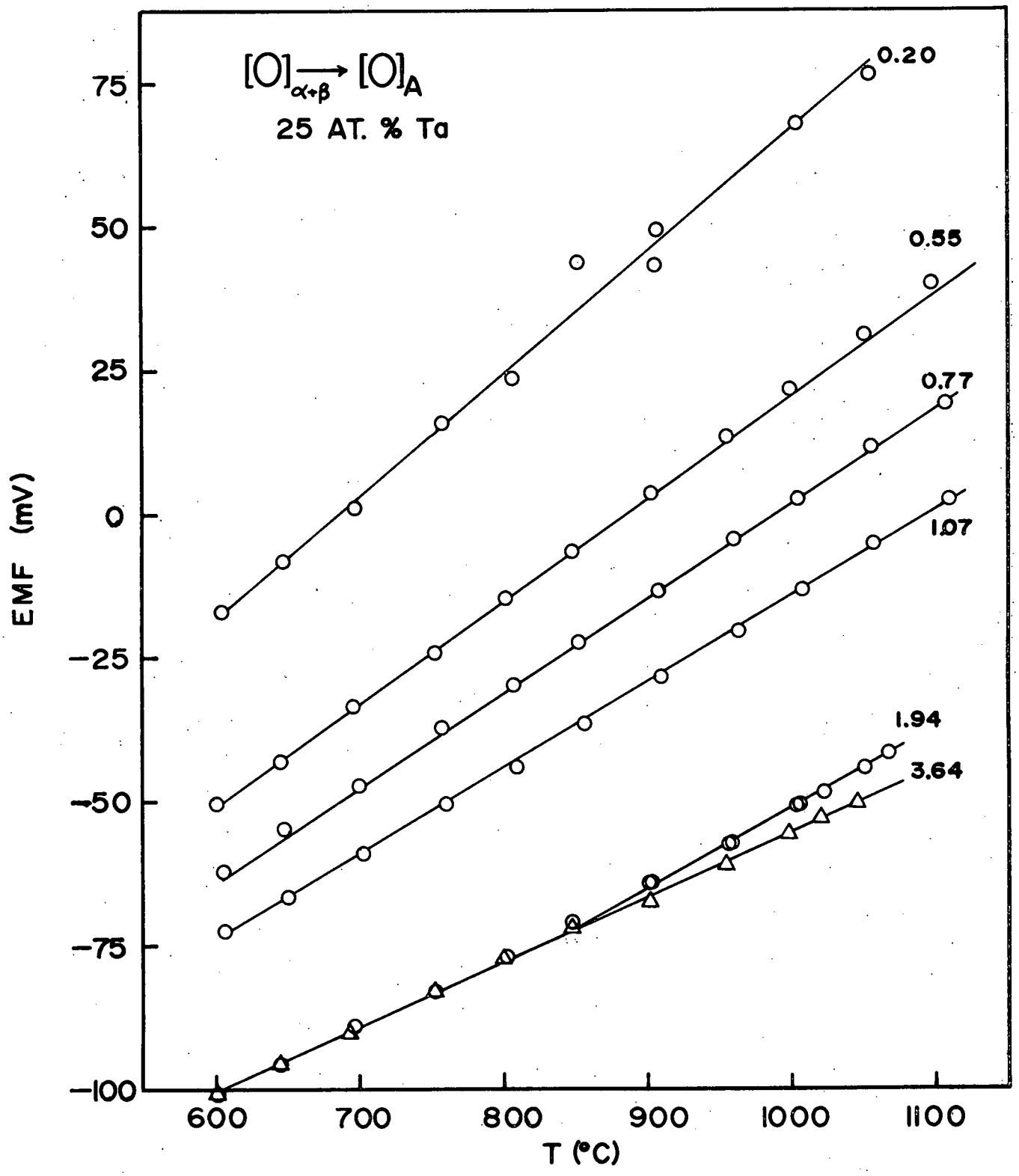

Figure 4: EMF versus temperature for the Nb-25%Ta alloy, relative to a two-phase vanadium/oxygen reference electrode. The small numbers on the right indicate the oxygen concentration in each specimen (in atomic %.)

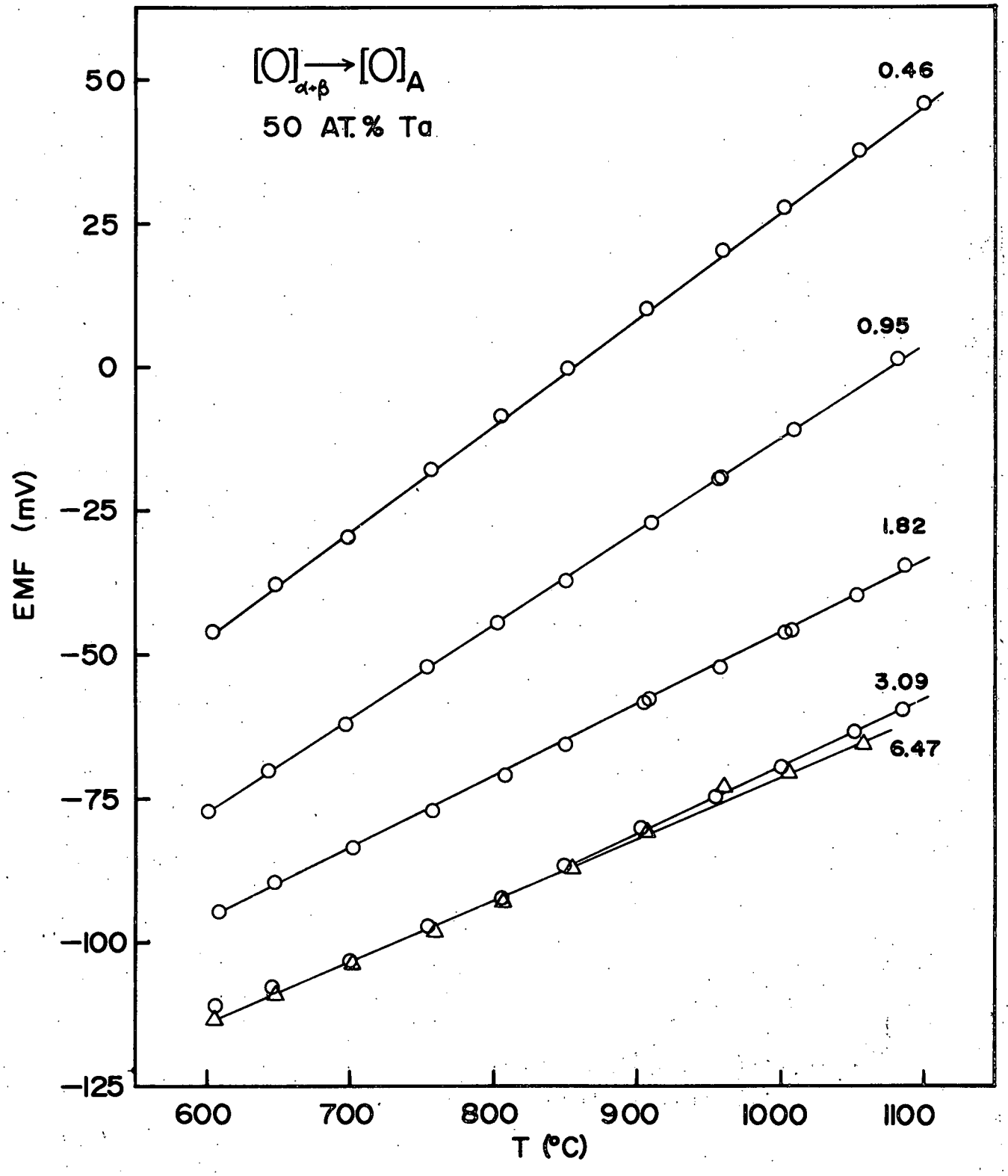

Figure 5: EMF versus temperature for the Nb-50%Ta alloy.

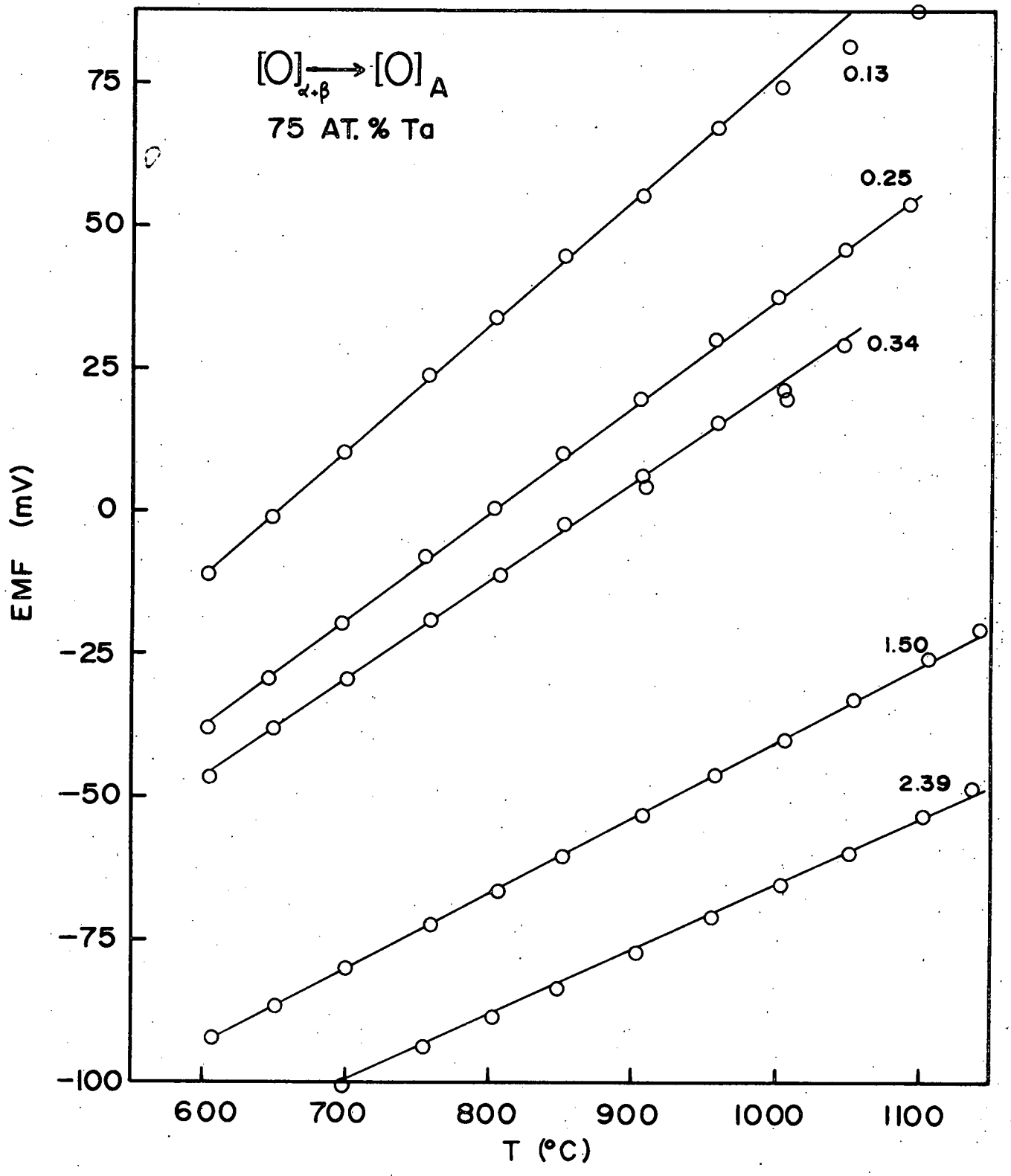

Figure 6: EMF versus temperature for the Nb-75%Ta alloy.

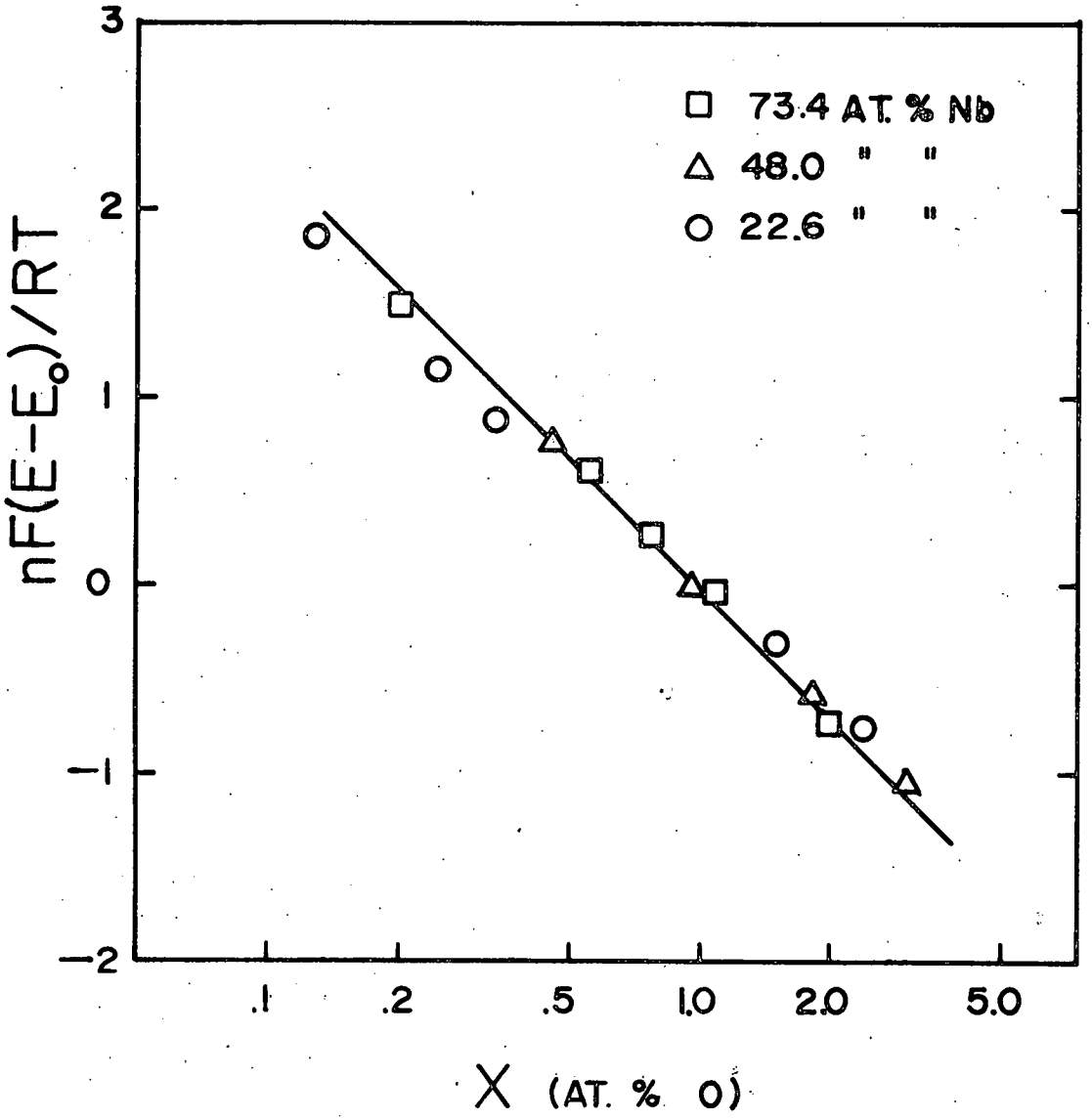

Figure 7: Henry's Law plot for the behavior of oxygen in the three niobium-tantalum alloys studied. The actual Nb:Ta contents are given in the upper right.

by interpolating the EMF(T) data to a 1 % solid solution. Figure 8 shows the resulting $\Delta G_1^o(T)$ for the three alloys. From these lines, the standard enthalpy and entropy changes, ΔH^o and ΔS^o, are calculated (as discussed in Section 2.5) and presented in Figure 9.

3.2 Oxygen Diffusion

3.2.1 Pure Niobium and Pure Vanadium

Figure 10 shows the result of a typical EMF run for oxygen diffusing in pure niobium. From the slope, dE/dt, the diffusion coefficient for oxygen is calculated at the particular temperature. The resulting data from several such runs are shown in Figure 11, along with the results of previous work reviewed by Boratto and Reed-Hill (29). A least-squares analysis of all data points results in the following expression for the "normal diffusivity" D_n:

$$D_n^{Nb}=(6.71 \times 10^{-3})\exp(-26380/RT) \quad cm^2/sec$$

Figure 12 shows the results of this study only, compared to the line calculated with the expression above. The scale is expanded to facilitate comparisons with the data for oxygen diffusion in substitutional alloys.

Similarly, the data for diffusion in vanadium are presented in Figure 13. A least-squares analysis of all the data gives the following result:

$$D_n^{V}=(1.56 \times 10^{-2})\exp(-29388/RT) \quad cm^2/sec.$$

Figure 14 shows the data from this study compared to the line calculated with the expression above.

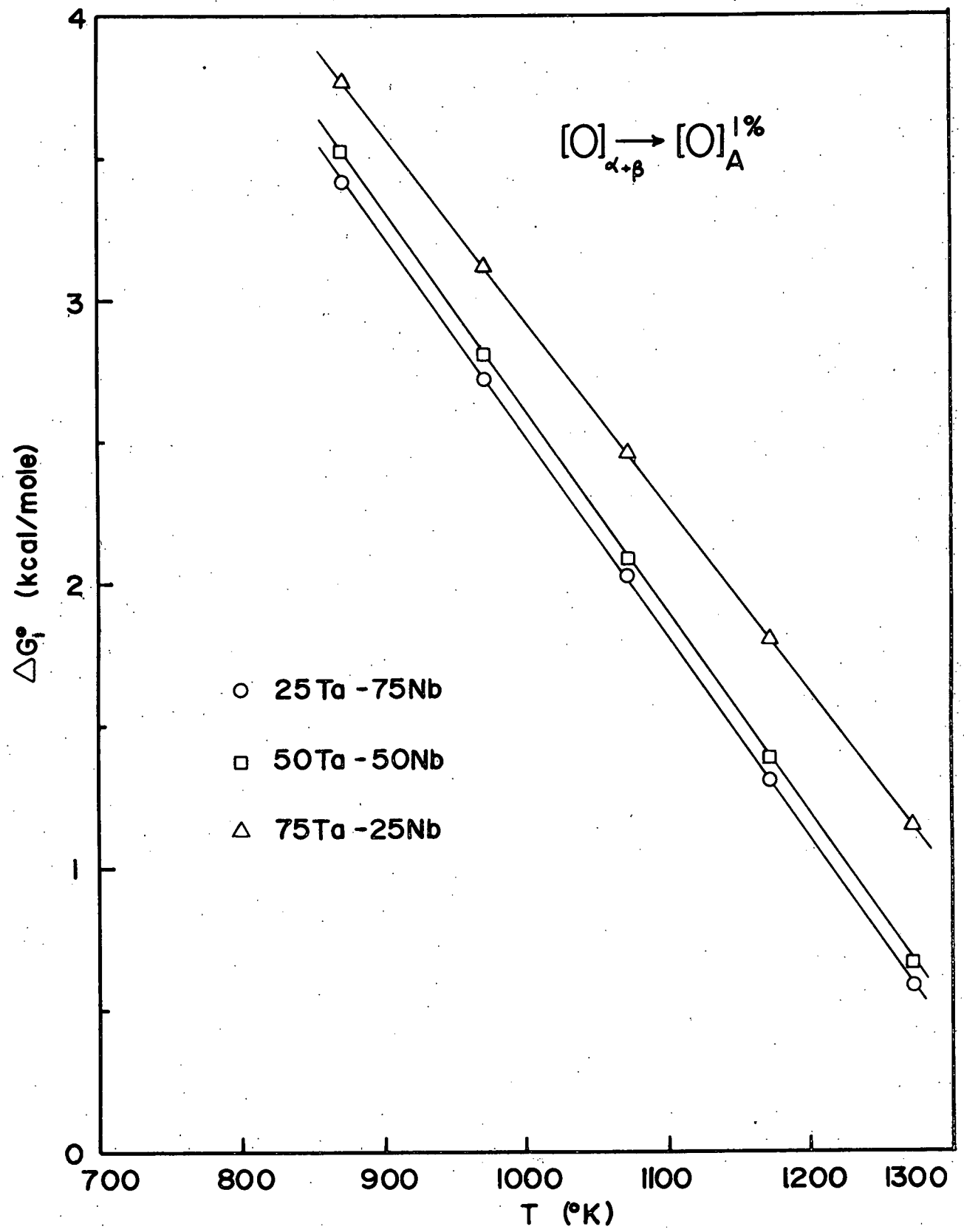

Figure 8. Standard free energy change for a 1 % solid solution of oxygen in each alloy, relative to the V-10%O reference electrode.

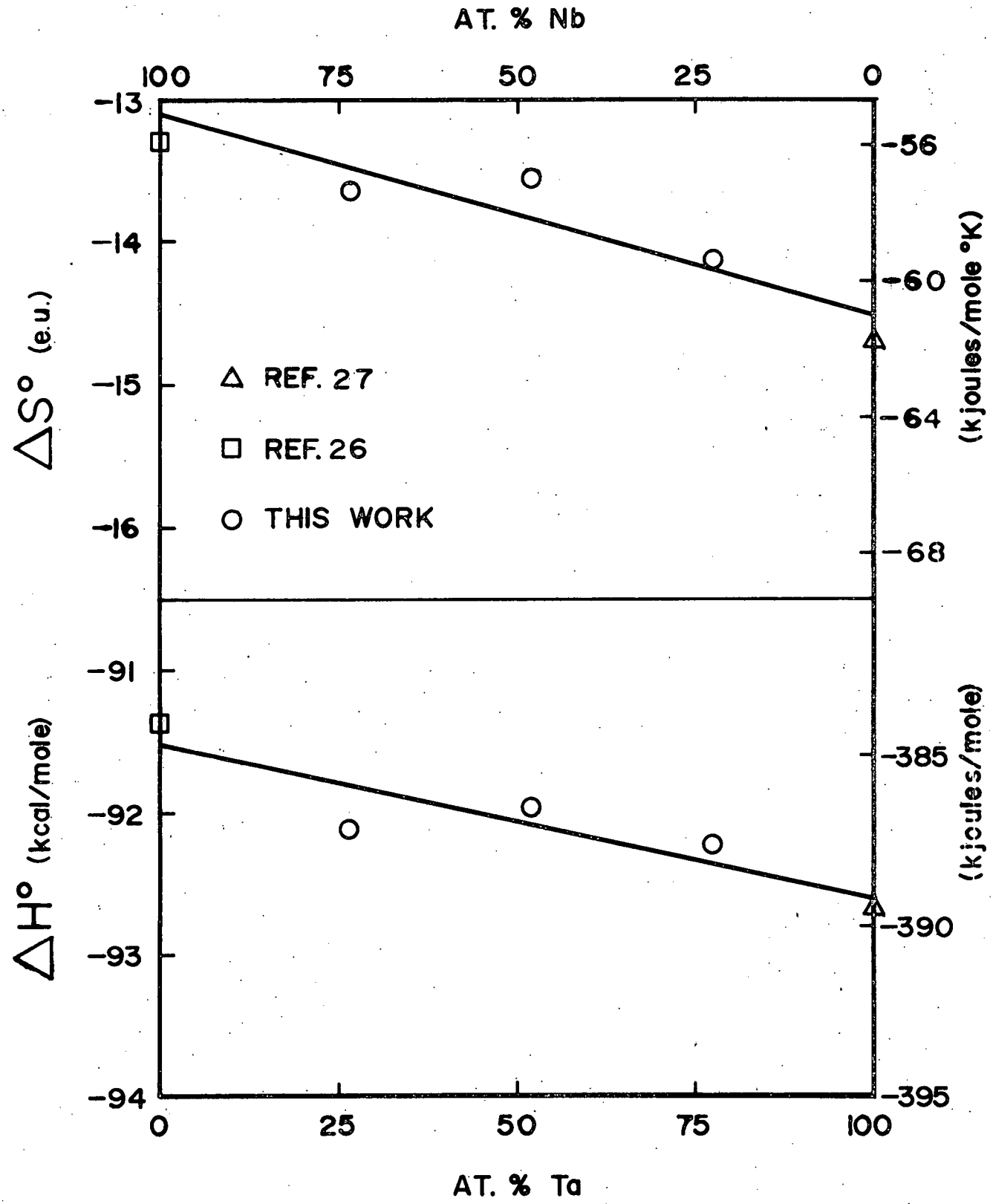

Figure 9: Standard entropy and enthalpy changes for the reaction $\frac{1}{2}O_2(g) \rightarrow [O]_A$ for a 1 % solid solution, as a function of Nb:Ta content of the alloy.

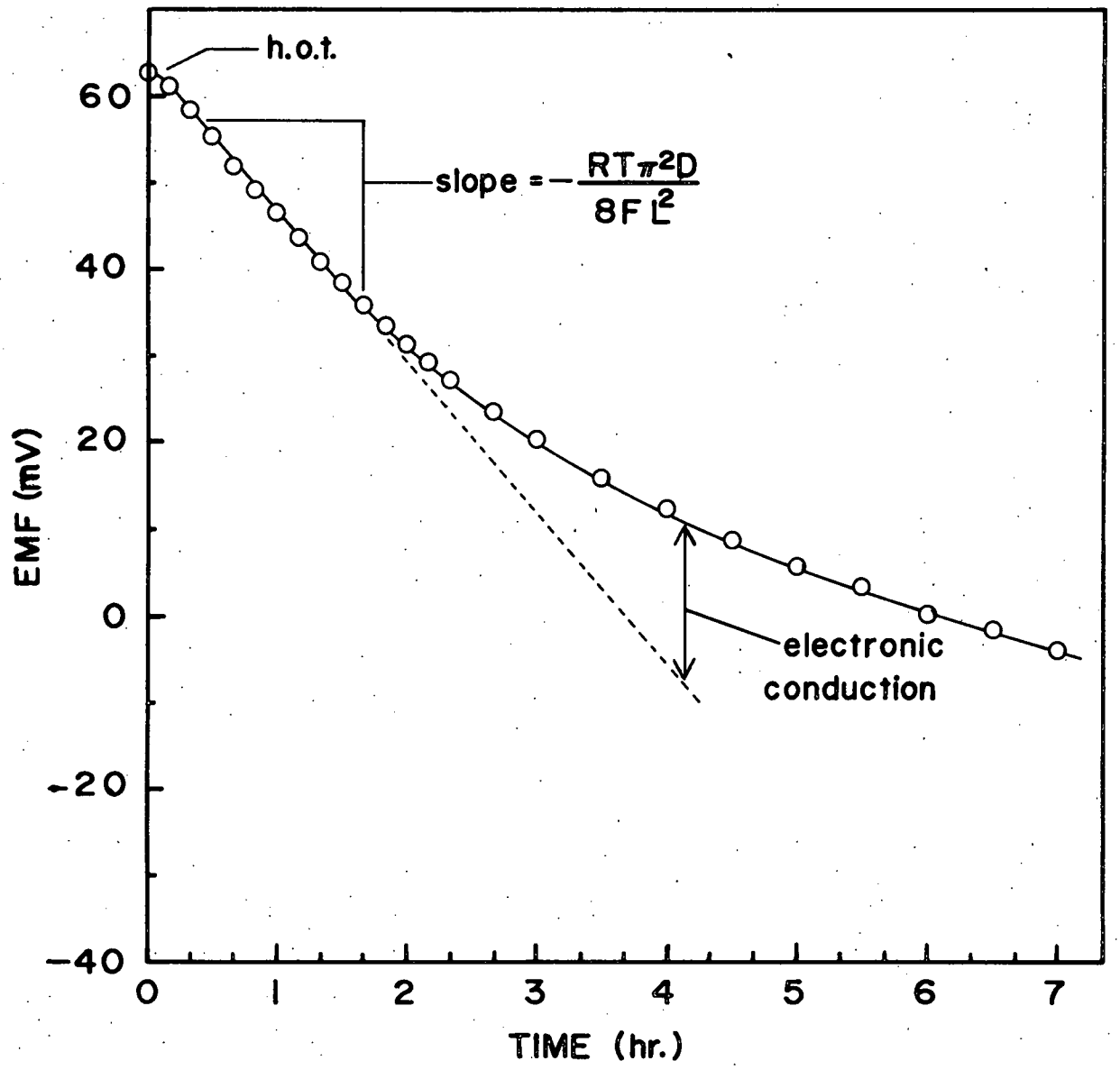

Figure 10: Typical plot of cell EMF versus time for Cell II; transient oxygen diffusion in pure niobium at 958°C.

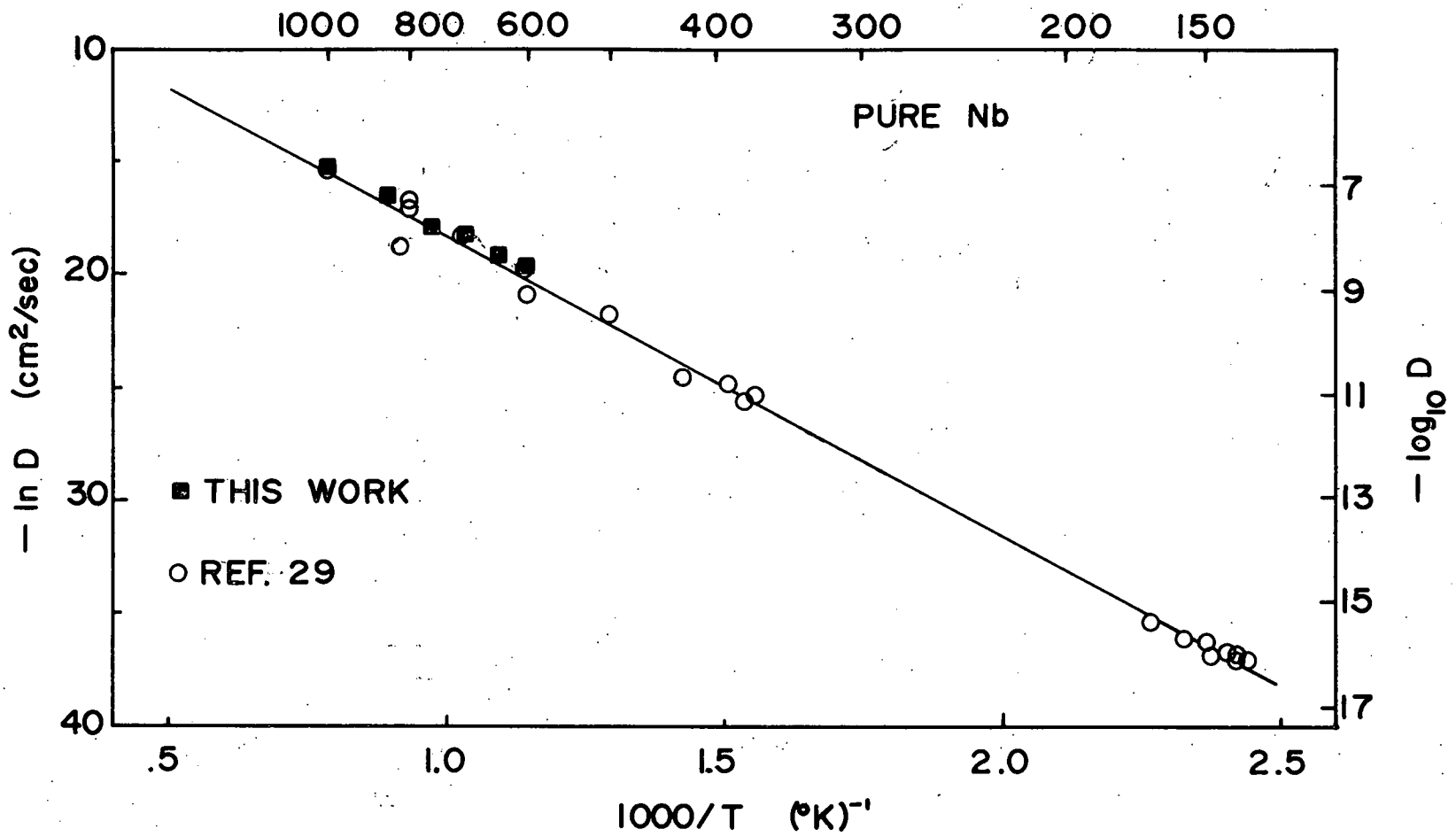

Figure 11: Arrhenius plot for the diffusion of oxygen in niobium.

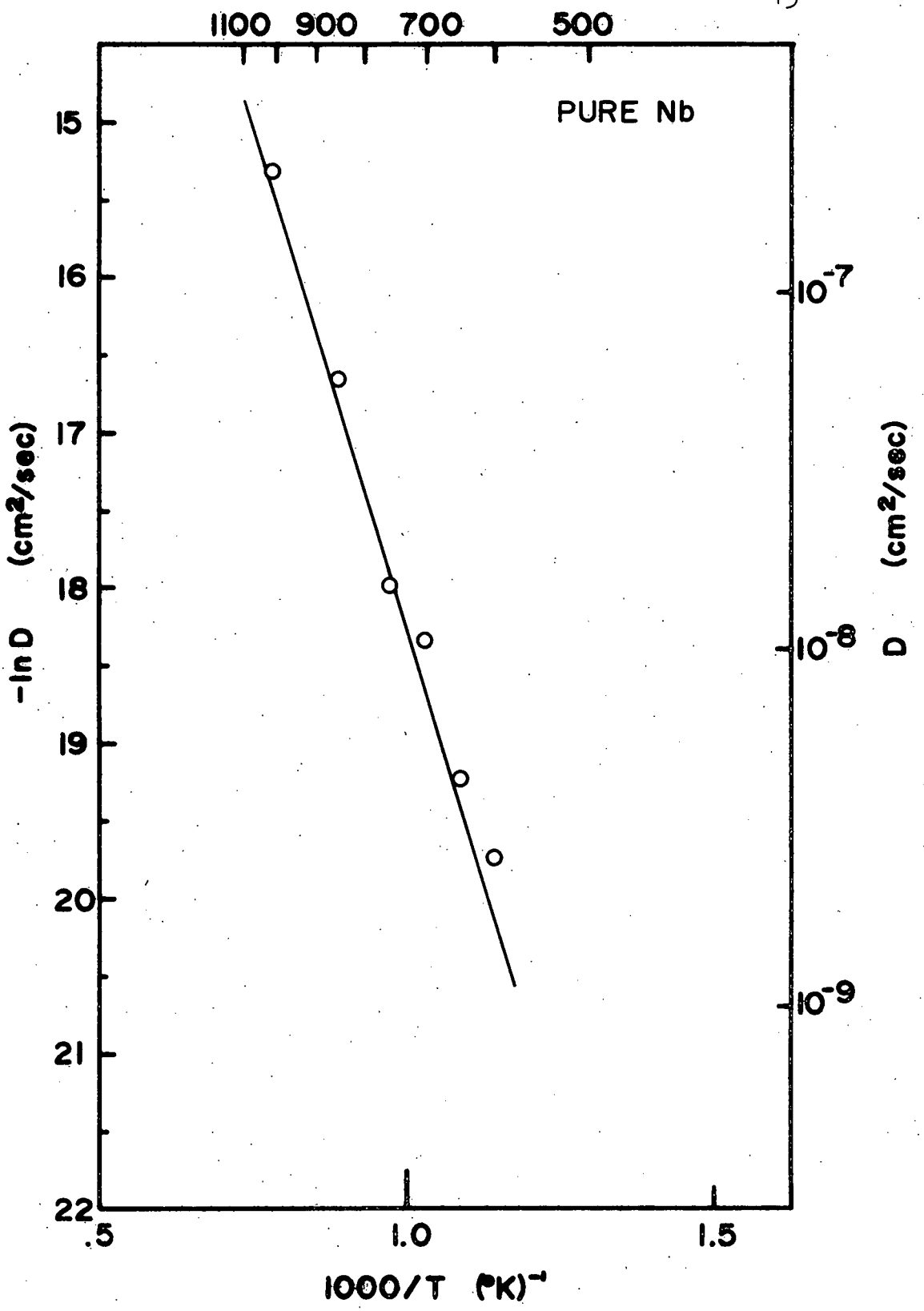

Figure 12: Arrhenius plot for the diffusion of oxygen in niobium (expanded scale.)

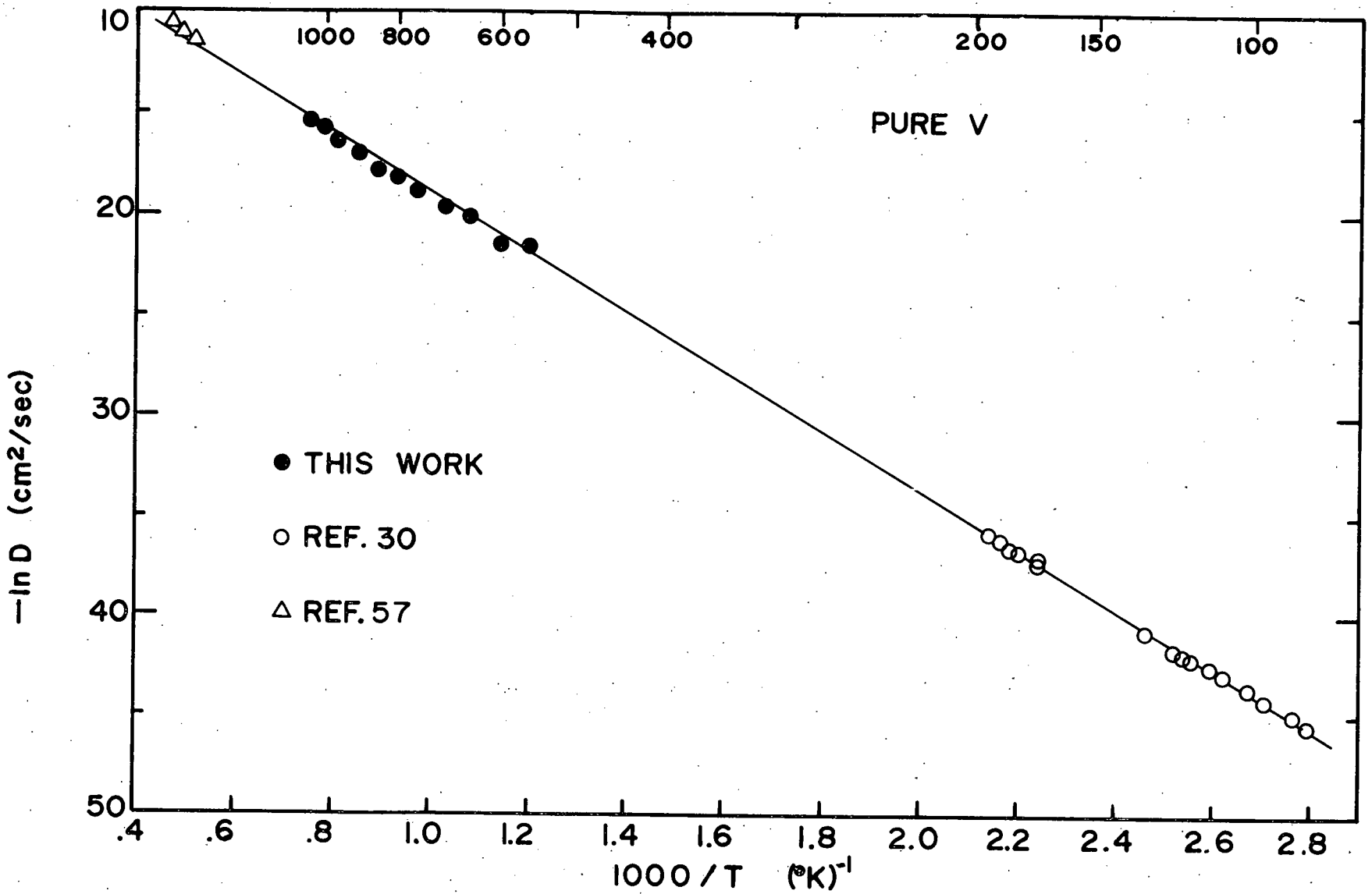

Figure 13: Arrhenius plot for the diffusion of oxygen in vanadium.

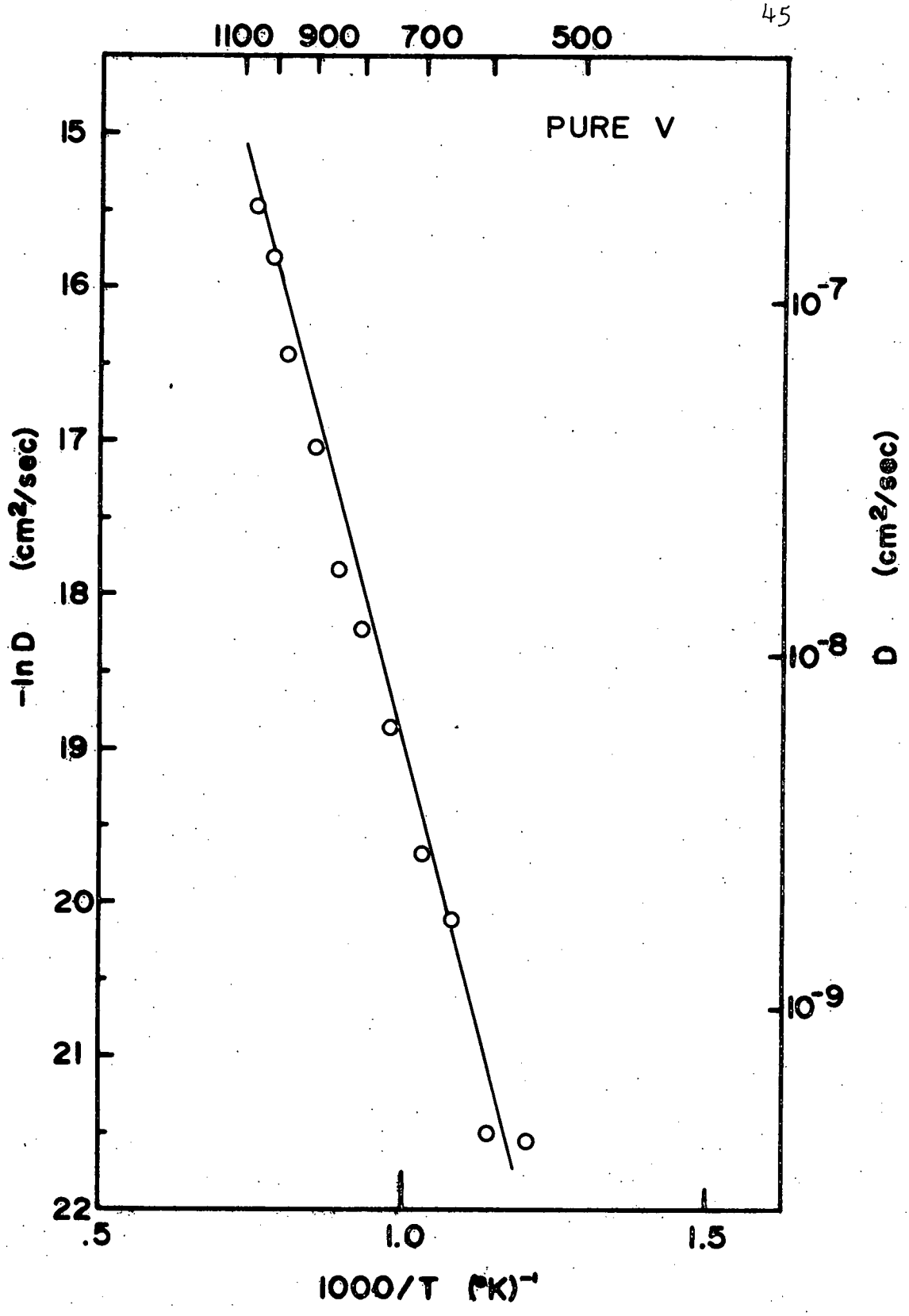

Figure 14: Arrhenius plot for the diffusion of oxygen in vanadium (expanded scale.)

3.2.2 Substitutional Alloys

Arrhenius plots for the diffusion of oxygen in the six substitutional alloys studied are presented in Figures 15 through 20. In each figure, the line corresponding to oxygen diffusion in pure niobium is shown for reference. For each alloy, several values of the trap energy were used to calculate expected values of D according to equation (7). The resulting lines are shown in each figure for comparison to the data. The values for the trap energy that give the best fit* to the data are summarized below:

TABLE III

Trap Energies for Substitutional Alloying Elements in Niobium (Oriani Model)

Element	Trap energy (eV)
Ta	0.3 ± 0.1
V	0.55 ± 0.05
Ti	0.7 ± 0.1
Zr	0.7 ± 0.05

*The data are considered within the framework of the Oriani model. Thus, the "best fit" in this sense is not the best fit in terms of a least-squares analysis.

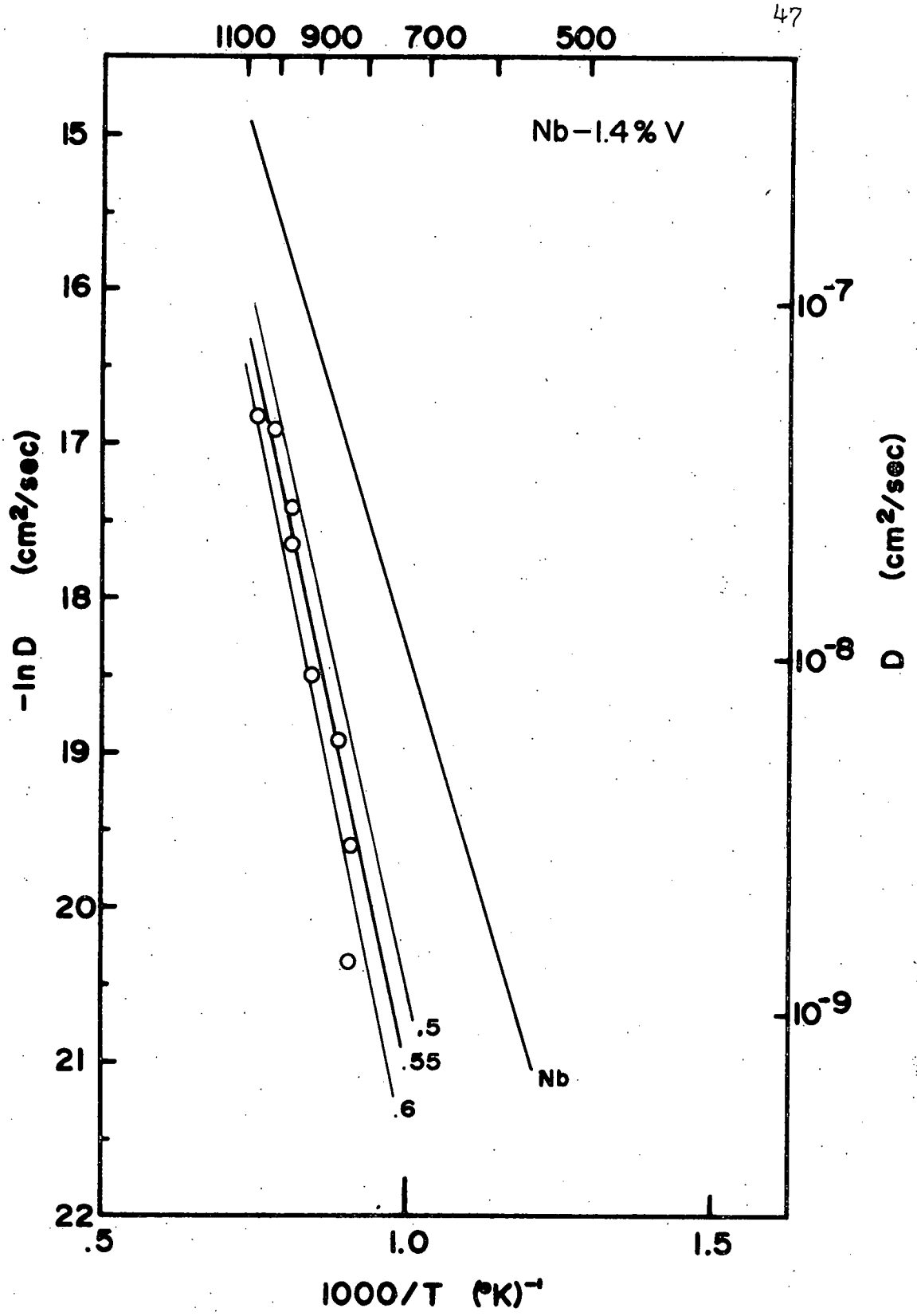

Figure 15: Arrhenius plot for the diffusion of oxygen in the Nb-1.4%V alloy. The line representing diffusion in unalloyed niobium is shown for reference. The small numbers are values of the trap energy, in eV.

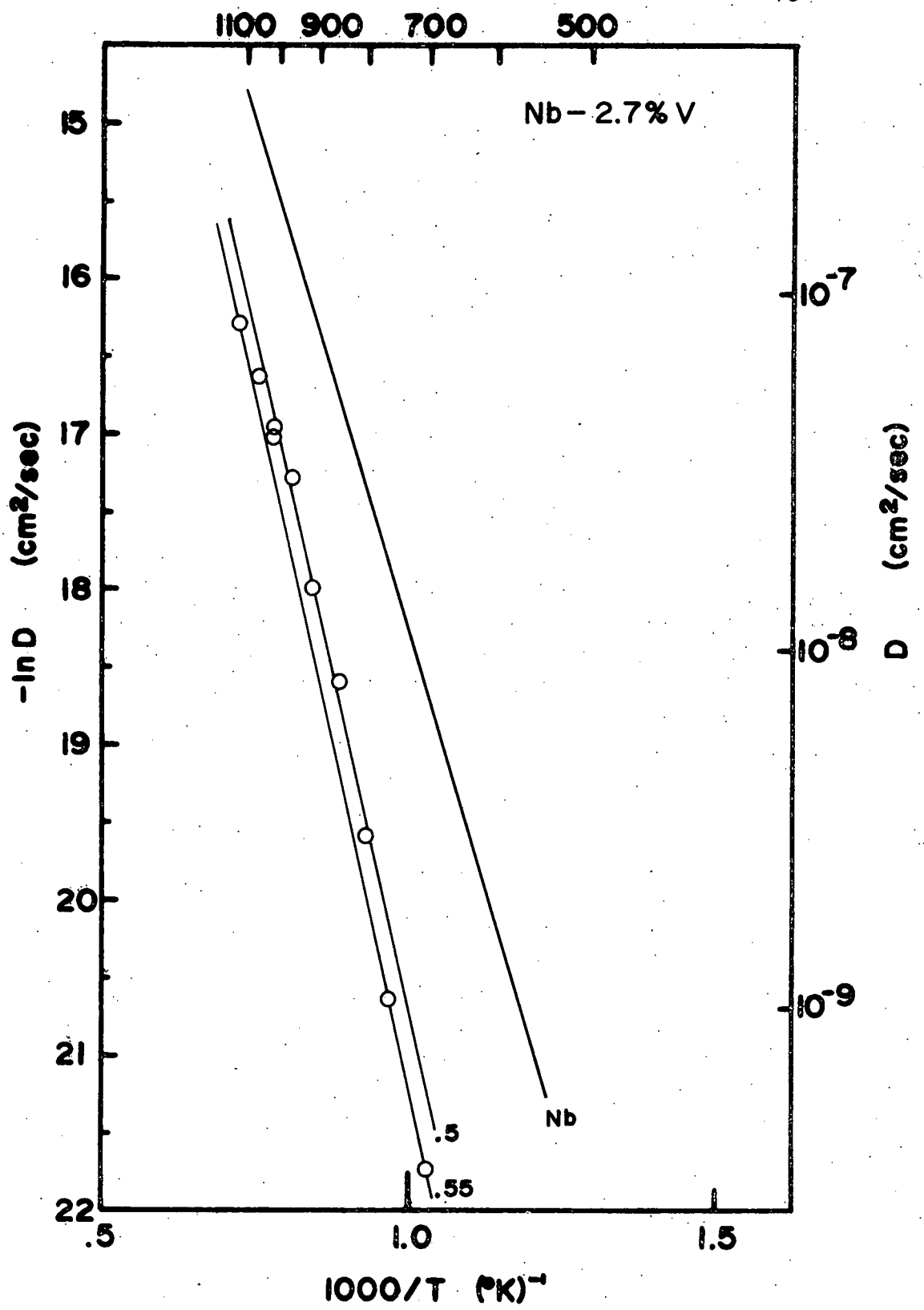

Figure 16: Arrhenius plot for the diffusion of oxygen in the Nb-2.7%V alloy.

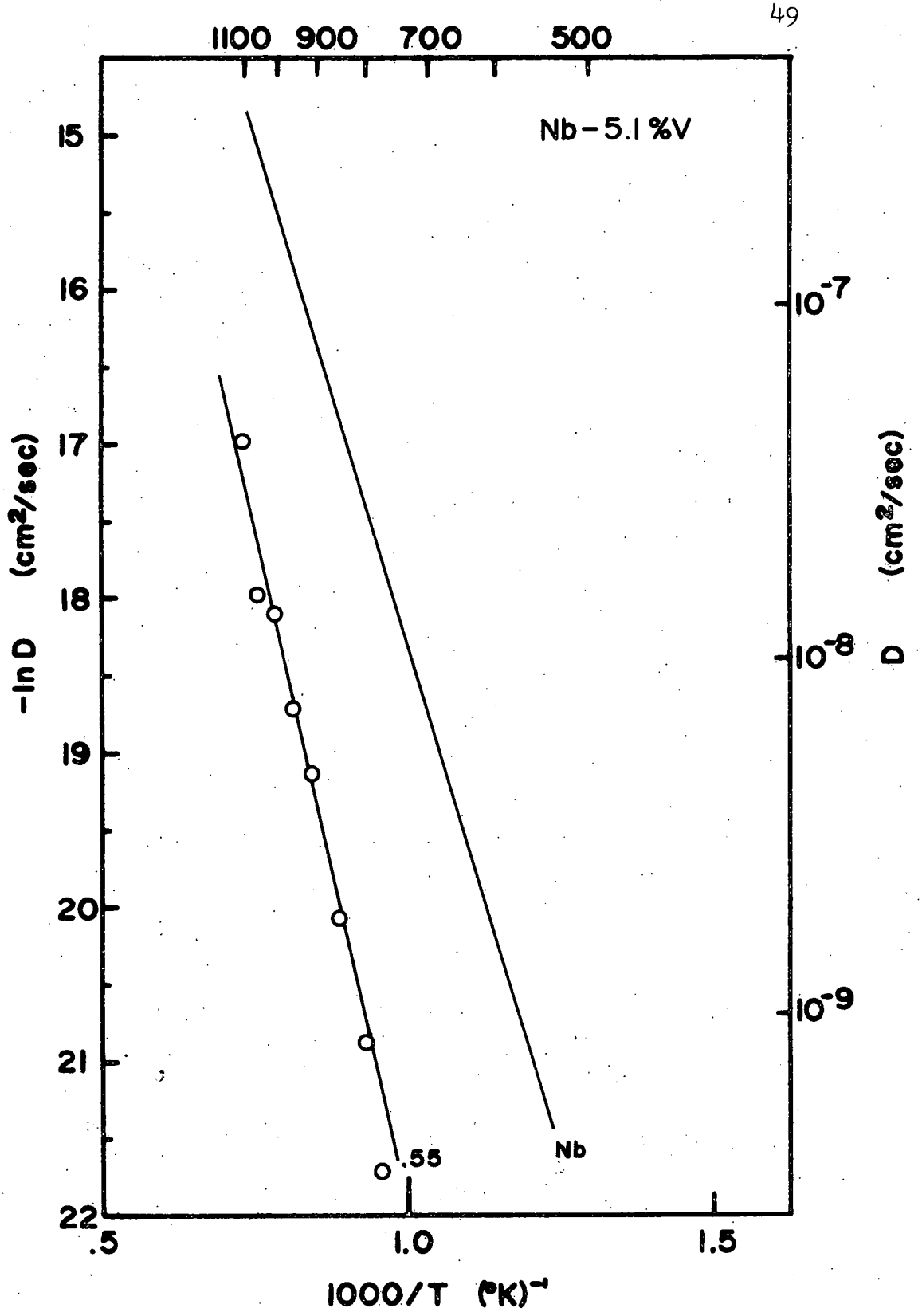

Figure 17: Arrhenius plot for the diffusion of oxygen in the Nb-5.1%V alloy.

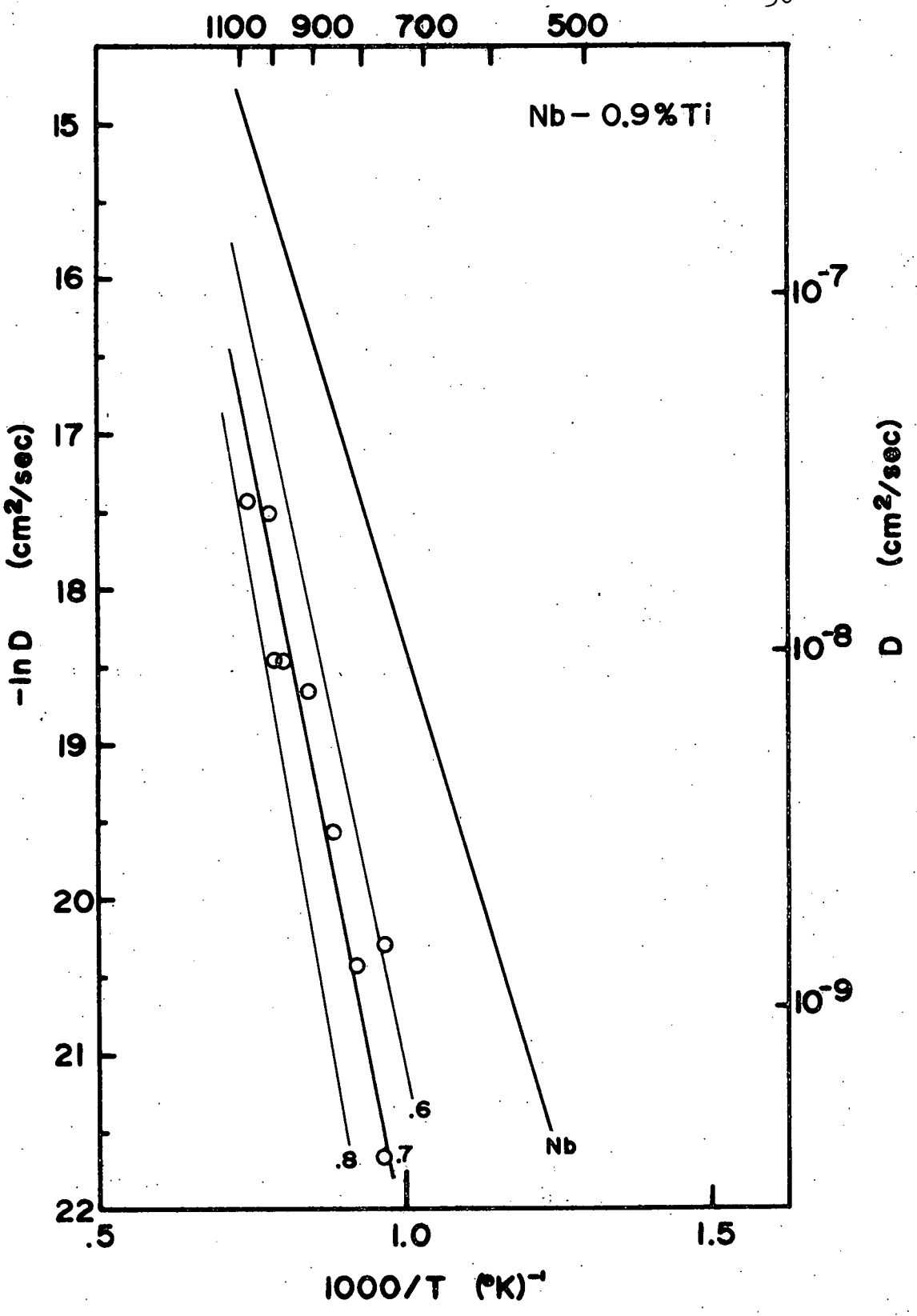

Figure 18: Arrhenius plot for the diffusion of oxygen in the Nb-0.9%Ti alloy.

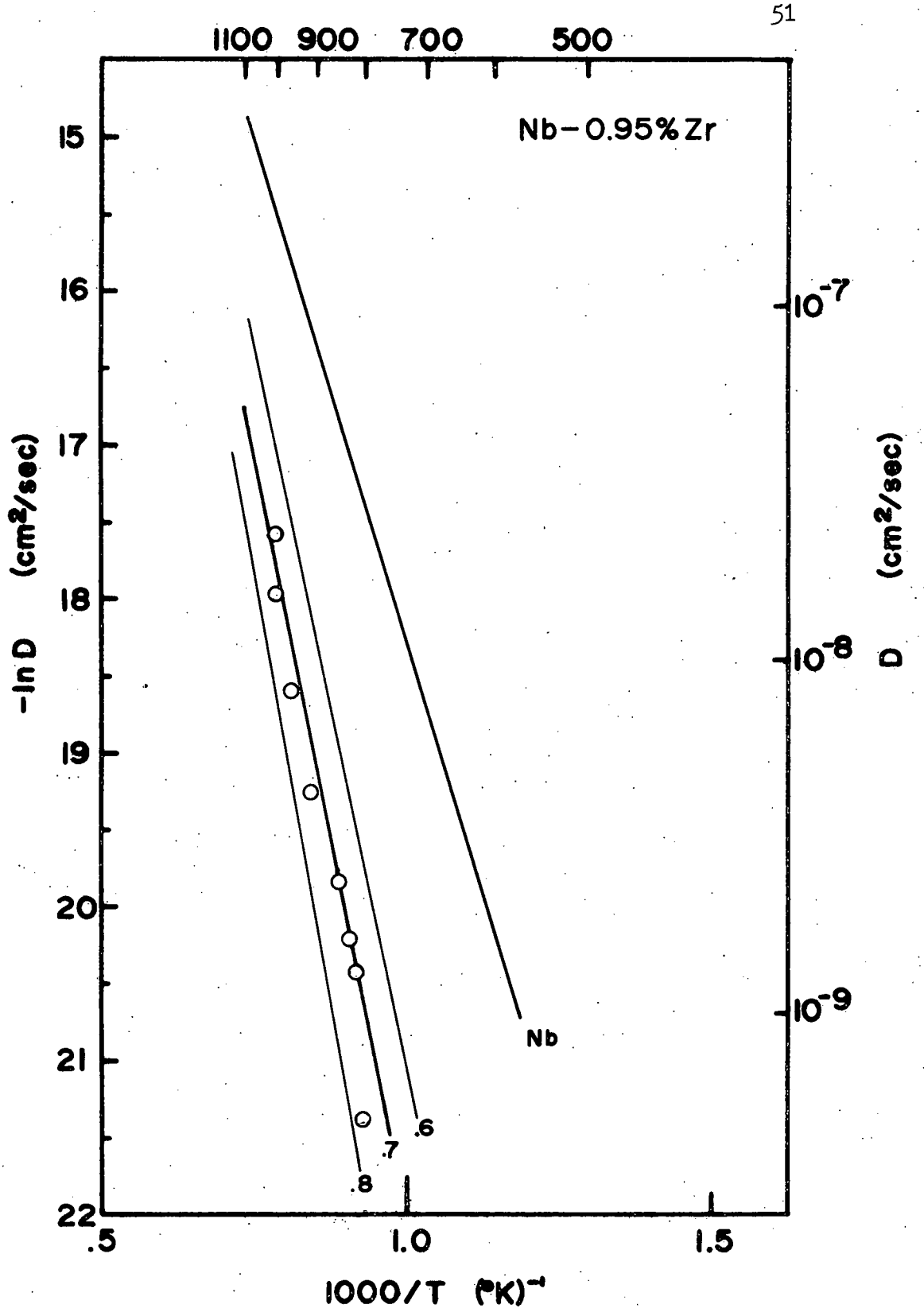

Figure 19: Arrhenius plot for the diffusion of oxygen in the Nb-0.95%Zr alloy.

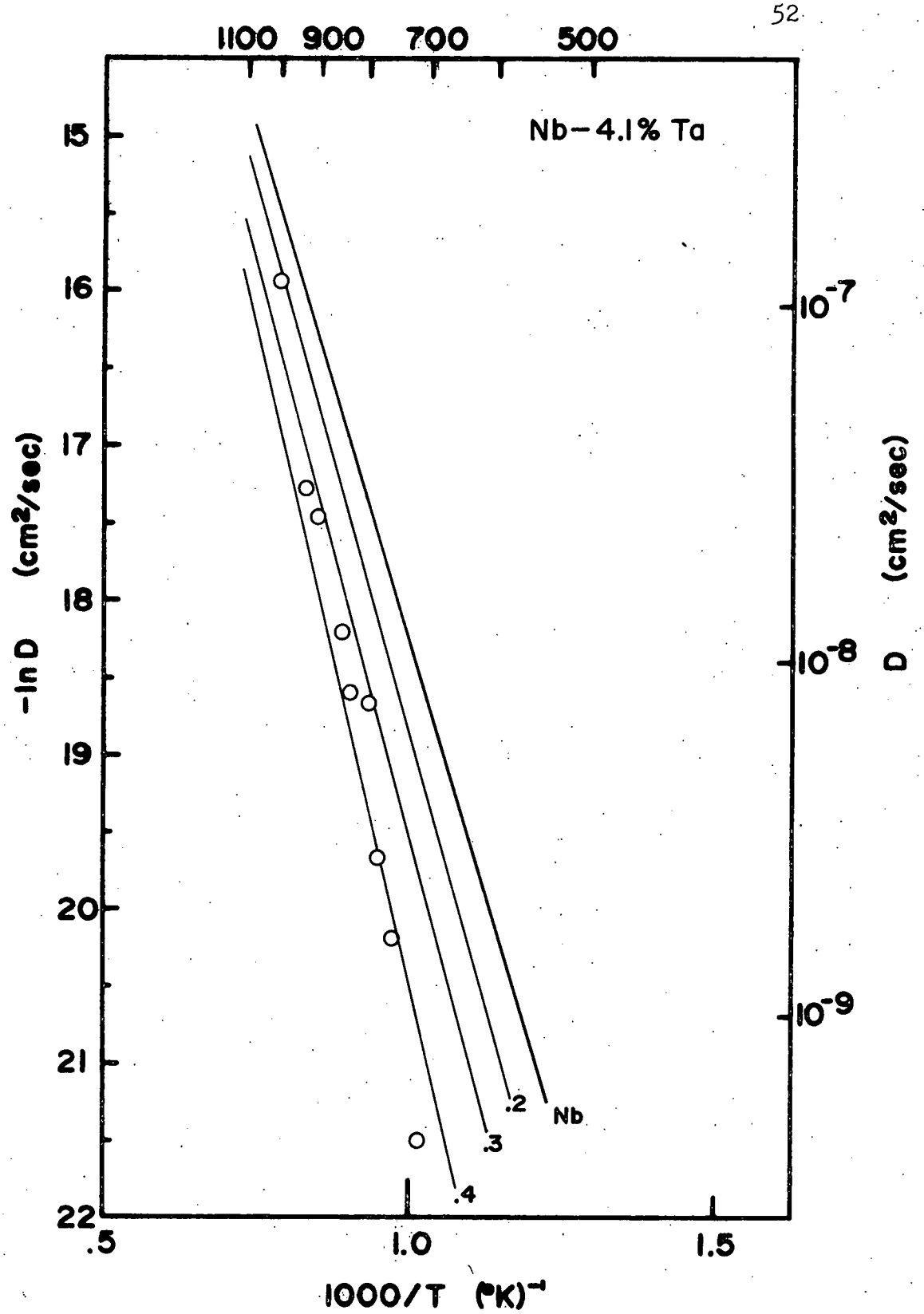

Figure 20: Arrhenius plot for the diffusion of oxygen in the Nb-4.1%Ta alloy.

3.2.3 Microhardness Measurements

It has been demonstrated (58) that the microhardness of a metal-oxygen solid solution can be related to its oxygen content. Thus, the hardness of a specimen in the as-doped condition could be compared to that of a specimen after an EMF run to verify that the oxygen actually did diffuse out of the specimen and into the zirconium block. A complete hardness traverse across the "used" diffusion couple should show the effect on the hardness of the zirconium due to the influx of oxygen.

Three alloys were chosen for microhardness testing. They were: Nb-2.7V-0.6O, Nb-0.9Ti-1.0O, and V-6.5Zr-O. In each case, a doped specimen that had never been in contact with an oxygen sink was mounted so that hardness readings could be taken across its thickness. A "used" specimen, with its zirconium block attached, was sliced perpendicular to the interface and mounted so that hardness measurements could be taken across the thickness of the entire diffusion couple. This is illustrated schematically in Figure 21.

The results are shown in Figures 22-24. In each case, the alloy in the as-doped condition is noticeably harder than the same alloy after diffusion has occurred.

The Nb-Ti-O alloy, Figure 22, has a hardness before diffusion of 200-240 DPH. (The scatter in the data is due to the fact that this specimen is probably two-phase at room temperature.) After diffusion, the hardness has fallen to a maximum, at the outer face, of about 160 DPH. The hardness decreases toward the interface, reaching a minimum value of about 100 DPH. The hard-

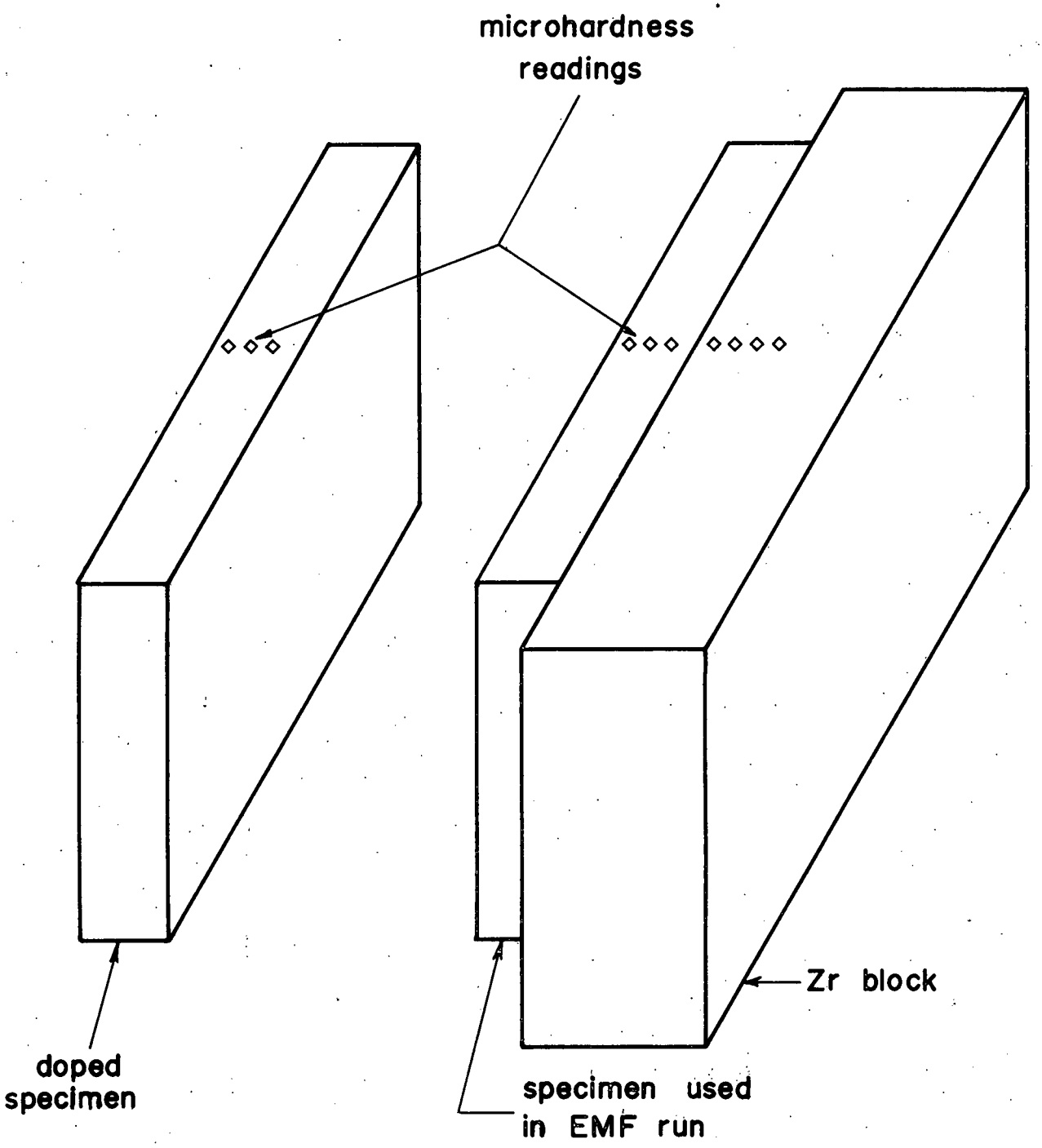

Figure 21: Schematic illustration of areas selected for microhardness measurements.

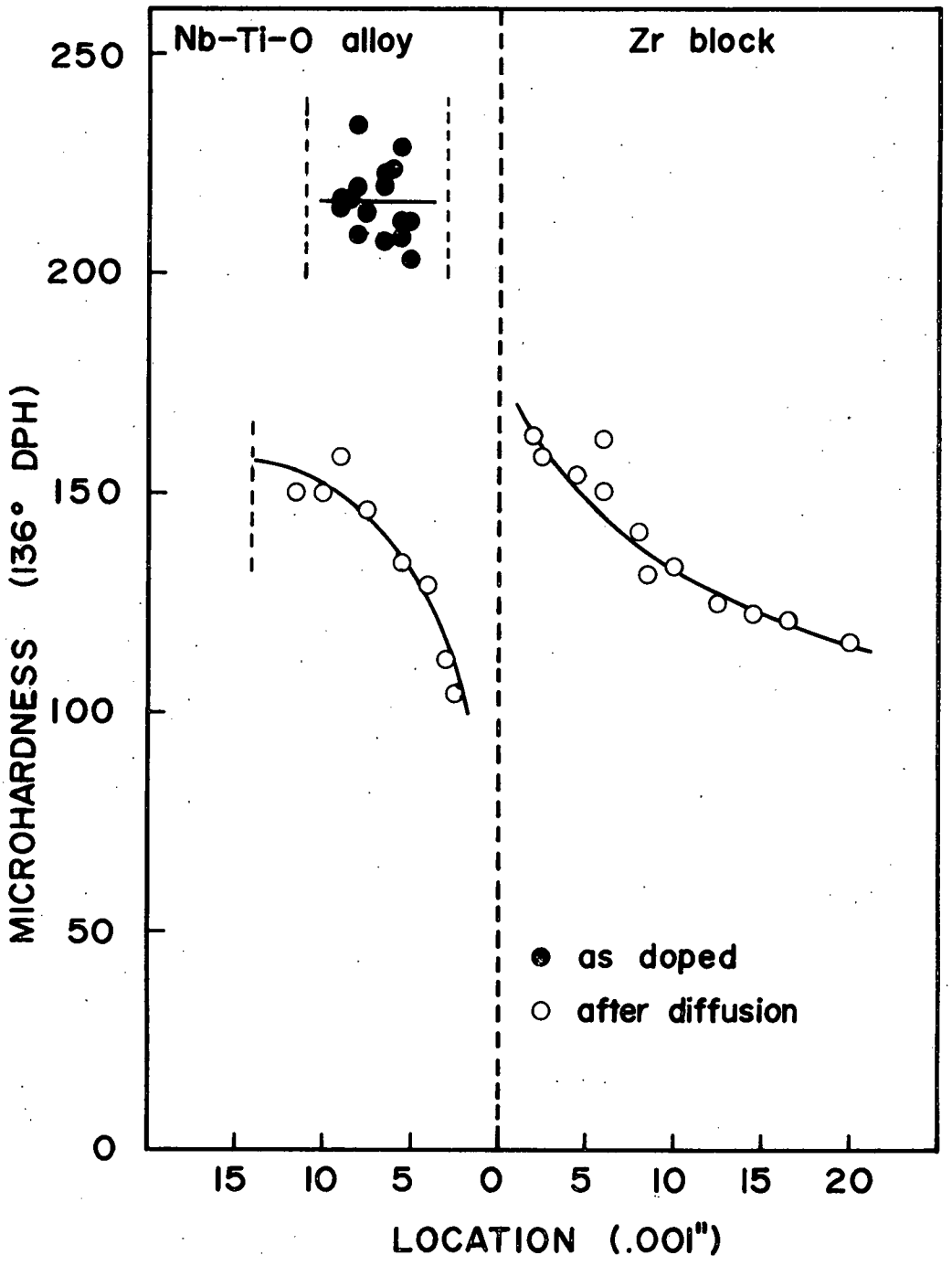

Figure 22: Microhardness of the Nb-0.9Ti-O alloy after doping with oxygen, and after contact with the Zr block.

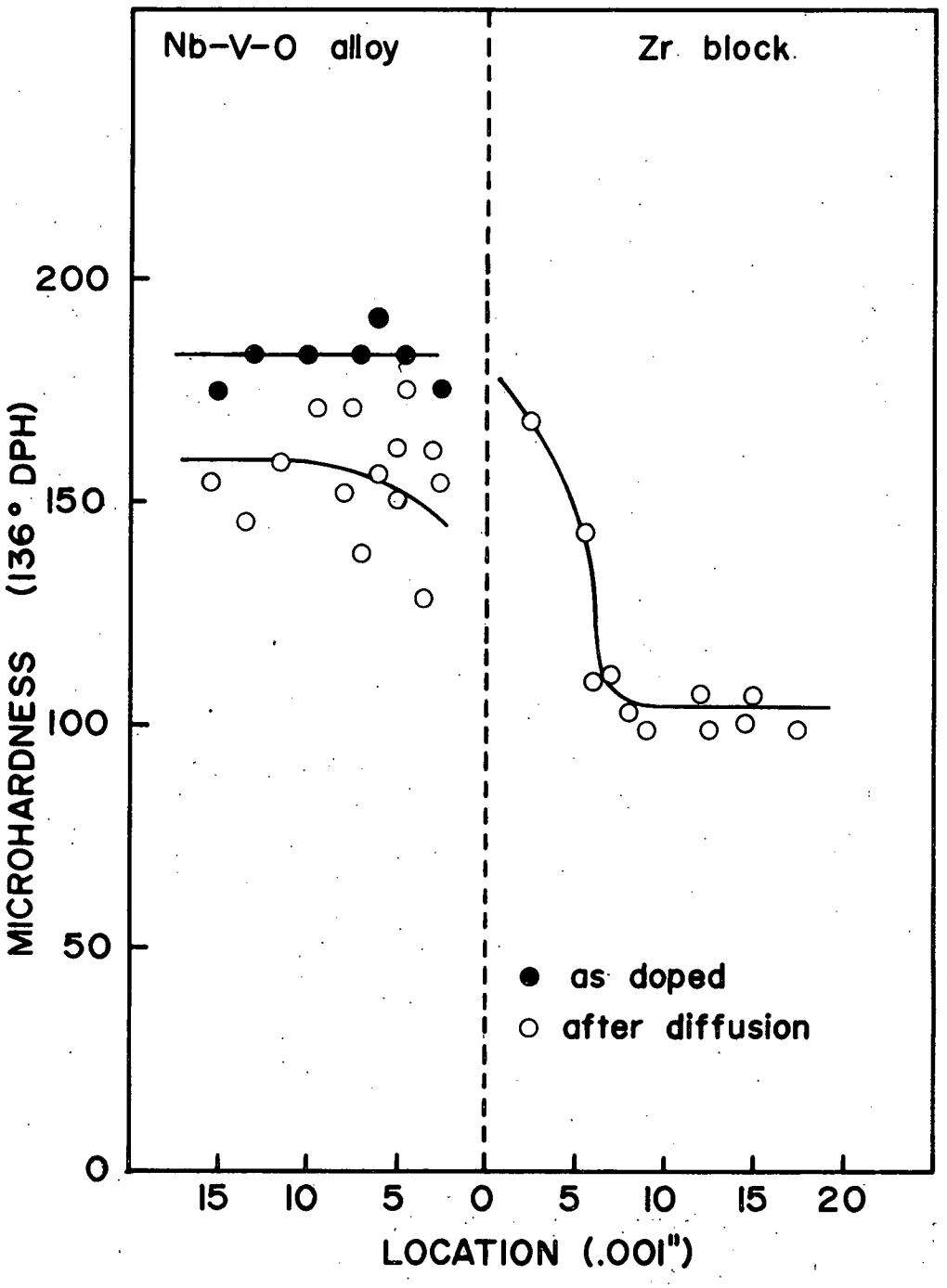

Figure 23: Microhardness of the Nb-2.7V-O alloy after doping with oxygen, and after contact with the Zr block.

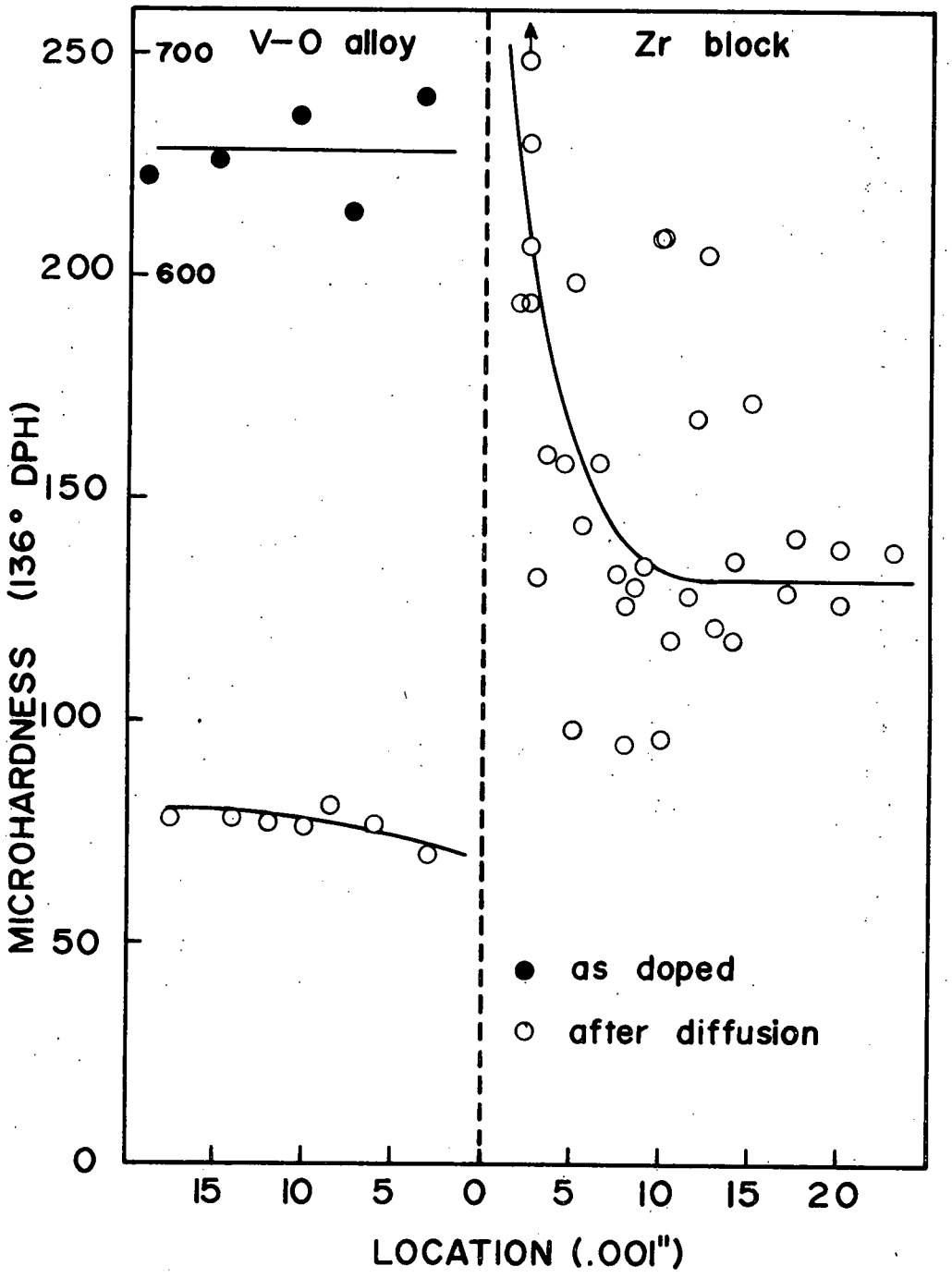

Figure 24: Microhardness of the V-6.570 alloy after doping with oxygen, and after contact with the Zr block. (Note the change of scale for the as-doped sample.)

ness of the zirconium block, on the other hand, reaches a maximum close to the interface (160-170 DPH) and decreases with distance from the interface.

The Nb-V-O alloy, Figure 23, shows the same general behavior as the Nb-Ti-O alloy, except that the decrease in the hardness due to diffusion is not nearly as great. This alloy, even after diffusion, was apparently two-phase at room temperature. The oxygen concentration gradient in the zirconium block is again quite visible.

The V-O alloy, Figure 24, shows the most striking decrease in hardness, from 600-700 DPH to approximately 75 DPH. The extremely high hardness in the as-doped condition is due to the fact that at 6 to 7% oxygen, the pure vanadium is a martensitic* phase. This diffusion couple was in contact at 950°C (1223°K) for approximately 100 hours. Because of the large amount of oxygen transferred, the overall hardness of the zirconium is greater in this specimen than in the previous two. Nonetheless, a clear trend of hardening toward the interface is apparent. (One point close to the interface had a hardness of 294 DPH, which put it off the scale of Figure 24, indicated by ↑.)

3.2.4 Auger Electron Spectroscopy

The three alloys that were tested for microhardness were repolished and examined in the Auger microprobe. For each alloy, one specimen was examined in the as-doped condition and one was examined after diffusion had occurred.

The Auger microprobe was operated in the following modes: a) imaging of specific elements, e.g., Nb, O, Zr; b) energy

*Formed on cooling to room temperature after doping.

scanning in selected areas (narrow raster); c) absorbed-current microscopy; and d) linear scanning to profile the distribution of a selected element.

Imaging the oxygen signal was difficult, due to the relatively low concentrations. In both the Nb-2.7V and the Nb-0.9Ti, after diffusion, the oxygen appeared to be most concentrated in a narrow region of the zirconium close to the interface. In the V-6.5$\underline{7}$O alloy, after diffusion, large second phases were present in the zirconium block.

The energy spectra of selected areas of each alloy, before and after diffusion, were compared to determine the amount of oxygen that had diffused into the zirconium from the alloy. To obtain semiquantitative results, the following method was used for each alloy:

An energy spectrum was determined in a small area on the as-doped specimen. A characteristic oxygen peak (usually 510 eV) was selected and its amplitude compared to that of a particular niobium or vanadium peak (197 eV and 437 eV, respectively). The resulting "amplitude ratio," AR, is compared to that of a specimen after diffusion. Then,

$$\frac{AR_{final}}{AR_{initial}} \cong \frac{C}{C_o} \qquad (37)$$

Table IV summarizes the amplitude ratios for the three alloys. It can be seen that in each case the zirconium has absorbed a substantial amount of oxygen from the alloy.

Figure 25(a) shows a typical absorbed-current image of the

diffusion couple. The vanadium specimen is on the left and the zirconium is on the right. The lighter areas in the zirconium are also visible optically and will be discussed in Chapter 4.

Figure 25(b) shows the same area as Figure 25(a). The relative concentration of each species is shown as a function of distance along the indicated line. It can be seen that the oxygen has been removed from the vanadium and is diffusing into the zirconium block. (The large noise level in the oxygen profile is due to the fact that the main oxygen peak was not usable due to interference from the vanadium. Therefore, a much weaker oxygen peak was used.)

TABLE IV

Results of Auger Electron Spectroscopy

Alloy	Oxygen/Metal Amplitude Ratio	
	As-doped	After diffusion
Nb-2.7V	0.12	0.09
Nb-0.9Ti	0.42	0.19
Pure V	0.72	0.09

3.2.5 Computer Simulation

The Nb-0.95Zr alloy was chosen for detailed analysis by the finite-difference method (as discussed in the Appendix).

For a given temperature, measured values were given for the specimen thickness, "normal" diffusivity, and trap concentration. Then, reasonable values were selected and assigned to the

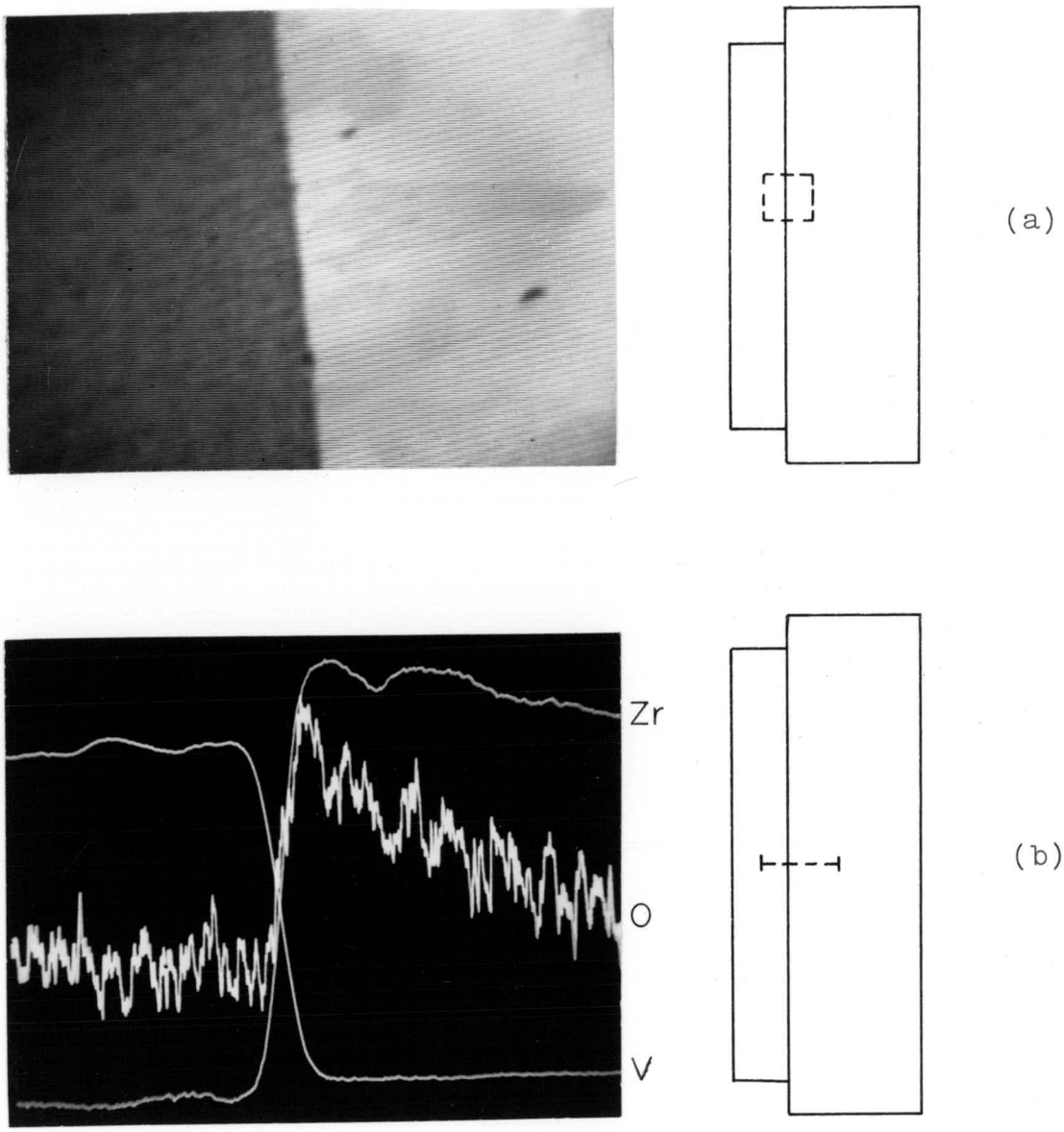

Figure 25: Auger photographs of the V-6.57O alloy, with Zr block attached, after 100 hours at 950°C.
(a) Absorbed-current image of interface region - zirconium is on the right.
(b) Zr, O, and V line scans.

trapping and release coefficients. Experimental data points for EMF(t) were put in for comparison. The computer program then solved the diffusion equations and presented the results as two calculated curves of EMF(t), one for simple diffusion and one for diffusion with trapping (59). The experimental curve appeared on the same plot for comparison. A typical output is shown in Figure 26. In addition, the equilibrium constant, K, relating trapped and untrapped concentrations, was calculated for a given pair of trapping and release coefficients.

If the slope of the computed EMF curve differed from that of the experimental curve, the trapping or release coefficient was changed and the process was repeated. Those values of the trapping/release coefficient ratio that gave the best fit to experiment are summarized in Table V and compared to results of calculations based on the Oriani Model.

TABLE V

Results of Finite-Difference Method
Compared with Those of Oriani Model

Temperature ^{o}K	$\frac{\text{Trapping coefficient}}{\text{Release coefficient}}$	Equilibrium Constant	
		Frank	Oriani
1088	6.59×10^{-21}	1100	1736
1101	6.88×10^{-21}	1148	1590
1125	6.34×10^{-21}	1057	1359
1178	5.60×10^{-21}	934	982
1231	4.60×10^{-21}	766	730
1273	3.73×10^{-21}	622	587
	Trap Energy	-0.4 eV	-0.7 eV

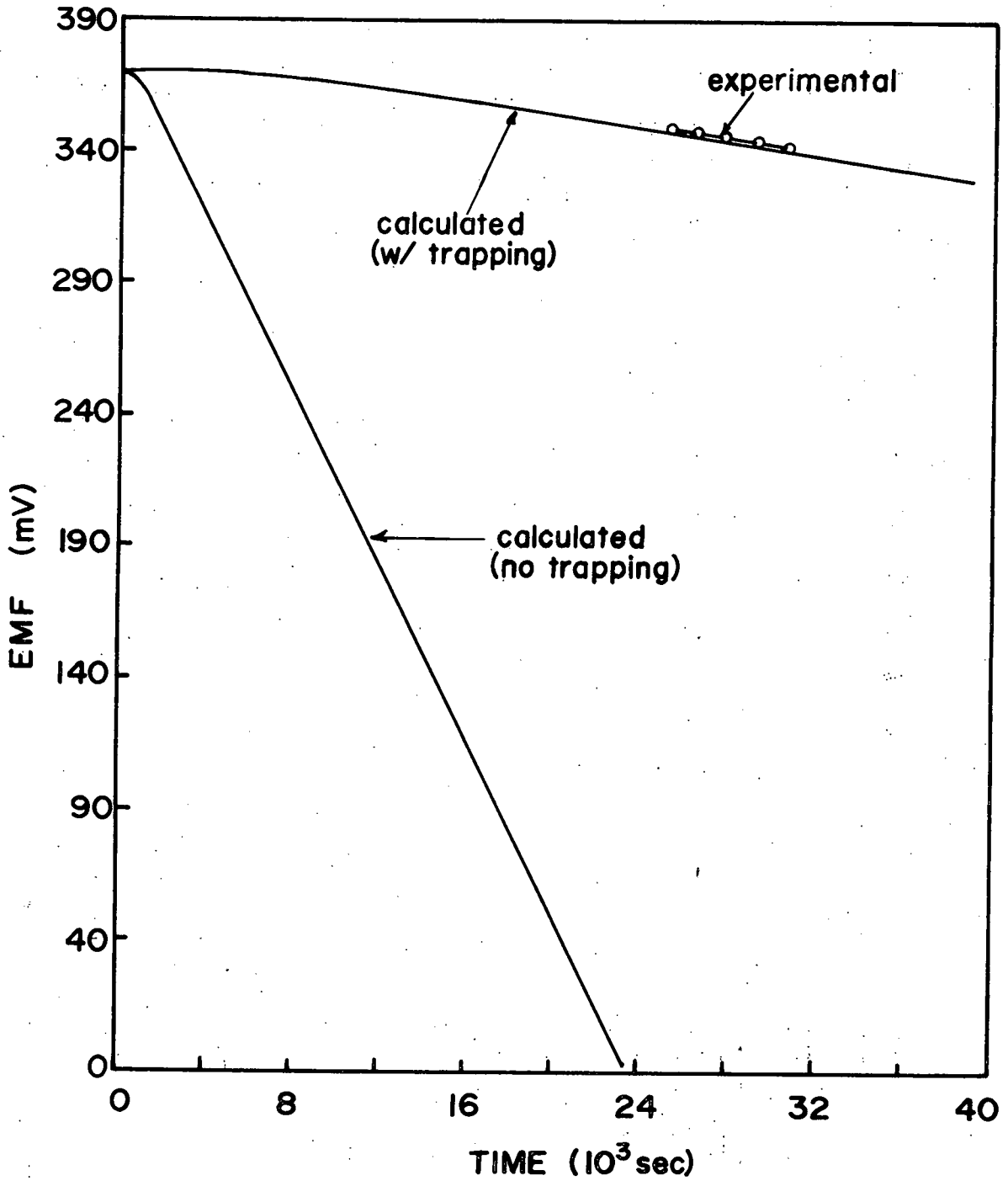

Figure 26: Typical output of computer simulation for transient diffusion of oxygen in Nb-0.95Zr. The EMF curve for simple diffusion (no trapping) is shown, along with the calculated and observed EMF(t) for trapping. The temperature for this plot is 1273°K.

4. DISCUSSION

4.1 Equilibrium in the Niobium-Tantalum-Oxygen System

4.1.1 Raw EMF Data

The raw EMF data, Figures 4-6, for all three niobium-tantalum alloys were quite consistent, and with only one exception (Nb-25Ta-0.2O) showed very little scatter. The data for Nb-75Ta-0.13O show the effect of electronic conduction which can occur at very high temperatures and low oxygen activities. In this case, the deviation from linearity became apparent at 1000°C and was proportional to the temperature increase above that point. It was also time-dependent.

The Nb-25Ta and Nb-50Ta data illustrate the EMF behavior when a solubility limit is reached. For the Nb-25Ta alloy, it may be concluded that below 850°C (1123°K) both the 1.94% and 3.64% oxygen samples are two-phase. Thus, both specimens have equal oxygen activities and hence equal EMF. It should be noted that 1.94% oxygen is not the true (equilibrium) solubility at 850°C, since the time required for precipitation of the equilibrium oxide phase would be very long. The oxide present in these samples no doubt has a composition corresponding to the Nb:Ta ratio of the matrix, which is not necessarily the equilibrium value for the oxide.

4.1.2 Thermodynamic Functions

Since oxygen obeys Henry's Law in pure niobium and tantalum up to the solubility limit in each, it is not surprising that it

also obeys Henry's Law in the ternary alloys, Figure 7. It is also not surprising that the standard entropy and enthalpy of formation of the 1% solid solutions vary almost linearly with Nb:Ta ratio, Figure 9. It is believed that in niobium-tantalum solid solutons the niobium and tantalum atoms are arranged randomly (60). The chemical properties of niobium and tantalum are similar, and their atomic radii are within 0.1% of each other.

The oxygen partial pressure in equilibrium with a niobium-tantalum solid solution containing oxygen can be expressed as follows:

$$P_{O_2} = X_O^2 \exp\frac{2}{R}\left[\frac{-389000+45.5X_{Nb}}{T} +60.9-0.055X_{Nb}\right]$$

where R is in joules/mole-^oK, X's are in atomic %, and P_{O_2} is in atmospheres. When an order-of-magnitude calculation is sufficient, the following expression gives the oxygen partial pressure (in Pa) at the temperature T (^oK) over niobium, tantalum, or niobium-tantalum alloys over the range 600-1100^oC:

$$\log X_O = \tfrac{1}{2}\log P_{O_2} + \frac{20200}{T} - 3.05$$

4.2 Oxygen Diffusion

4.2.1 Raw EMF Data

The measurements were taken over a temperature range of 600-1150^oC (873-1423^oK). The EMF curve that had the greatest slope represented diffusion of oxygen in pure niobium at 1000^oC. Its slope, dE/dt, was -1.13 X 10^{-2}mV/sec and corresponded to D_n=2.25 X $10^{-7}cm^2$/sec. The curve that had the slowest rate of change represented diffusion in the Nb-2.7V alloy at 696^oC (969^oK).

Its slope was -1.93×10^{-5} mV/sec and corresponded to $D=3.56 \times 10^{-10}$ cm^2/sec.

To accurately measure values of dE/dt that varied over three orders of magnitude, the frequency of data collection varied from once every ten minutes to once every four hours. In general, the curves formed fairly straight lines after allowing an initial period for the cell to establish equilibrium at each new temperature. Occasionally, the onset of electronic conduction would introduce a slight curvature to the line. This problem was minimized by taking the highest-temperature points first; then, when the oxygen activity was lowest, the cell would be at a more moderate temperature. Several specimens were used for each alloy, and doubtful points on the Arrhenius plots were retaken with another specimen whenever possible.

4.2.2 Arrhenius Plots

The points on the curves of $\log_e D$ versus $1/T$ showed no hysteresis, even though they were taken in a skipping fashion (i.e., 1000, 800, 950, ... etc.) Thus, over the range of oxygen concentrations studied, the diffusivity of oxygen is independent of oxygen concentration, in agreement with the observations of Perkins and Padgett (34).

The data for the diffusion of oxygen in niobium and vanadium are well-represented by straight lines. The agreement between the values reported in the literature (29,30) and those determined in this study is excellent. This is convincing evidence in support of the assumption of nearly perfect oxygen removal by the zirconium block.

The data for the six substitutional alloys are fairly well-represented by straight lines, although there is more scatter present in the alloy data than in the data for the two pure metals. There are two reasons for this: a) The reactive solutes, Ti and Zr, lowered the oxygen activity so drastically that electronic conduction was more of a problem in these alloys than in niobium or vanadium, particularly at the higher temperatures. b) At the lowest temperatures, diffusion in the alloys was so slow that it was sometimes difficult to measure dE/dt accurately.

Oxygen diffusion in each of the alloys was slower than diffusion in niobium at the same temperature. In some cases, the diffusivity was lowered by more than an order of magnitude. This overall effect is many times greater than the relative error of the individual data points.

The data for Nb-2.7V and Nb-5.1V have a very slight curvature. However, since all of the data points fall within a relatively narrow error band, it was decided not to attempt any non-linear curve fitting for these alloys. It is significant to note that, using the Oriani model, all three Nb-V alloys give the same value for the O-V binding energy (-0.55 ± 0.05 eV). Thus, it appears that the two-state model is valid to at least 5% substitutional content, although the upper limit is probably not much higher.

The Arrhenius plot for diffusion in Nb-4.1Ta does not follow a line calculated by the Oriani model as well as do the data for the other alloys. This is discussed more fully in the following section.

4.2.3 Application of Theoretical Models

1. Oriani: The model predicts Arrhenius plots which appear to represent the data fairly well, with the exception of Nb-4.1Ta. The same O-V binding energy was indicated by the data for each of the three different Nb-V alloys studied. The method of analyzing the data according to the Oriani model takes the following form:

(equilibrium) $$K=\frac{1}{\theta_n}\left[\frac{\theta_x}{1-\theta_x}\right] \qquad (6)$$

(oxygen mass balance) $$3N\theta_n+3N\cdot 2X_s\theta_x=NX_0$$

where X_s = atom fraction substitutional solute

X_0 = atom fraction oxygen (X_0=0.005 was used.)

$$K = \exp(-\Delta E_x/kT) \qquad (8)$$

A value of ΔE_x was chosen, and K was calculated at some temperature. An expression for θ_n in terms of θ_x (obtained from the mass balance) was substituted into equation (6) and the resulting quadratic equation was solved for θ_x. The value of θ_n was calculated from the oxygen mass balance. Then,

$$D=D_n\frac{\theta_n}{\theta_n+2X_s\theta_x(1-\theta_x)}$$

gives the "predicted" D at the given temperature. When this calculation is performed for several temperatures, an "Arrhenius" line is obtained for constant ΔE_x. If this line does not represent the data, a new value of ΔE_x is chosen and the procedure is repeated.

The assumptions are that ΔE_x is not a function of oxygen

concentration, substitutional concentration, or temperature. These assumptions appear to be valid for all solutes studied except tantalum. The data for Nb-4.1Ta can be closely approximated by a straight line, but it is definitely not any line predicted by the Oriani model for constant trap energy.

Two possible explanations are:

a) The trap energy may be a function of temperature. To explore this more fully, Figure 27 shows the result obtained with the Oriani model, modified so that:

$$\Delta E_x = (1.3 \times 10^{-3})(T-1370) \qquad \text{for } 1370 < T < 1070^{\circ}K$$

It can be seen that this calculated curve fits the data fairly well. This emphasizes the important point that the trap energy may, in some cases, have an entropy contribution. The Oriani model assumes that the only entropy change is configurational. If, however, there are other entropy contributions, then the exponential in equation (8) could be temperature-dependent.

b) Tantalum and niobium are chemically similar, and are the same size. Thus, tantalum may form such a weak trap that longer-range effects become apparent (e.g., changes in the elastic properties of the alloy as a whole). This overall effect may be small enough to be masked by stronger traps, such as Ti or Zr.

Clearly, future work should include a re-examination of this alloy, and other dilute Nb-Ta alloys, to gain a better understanding of their behavior. Until more data are obtained for this system, it seems most appropriate to treat this particular alloy

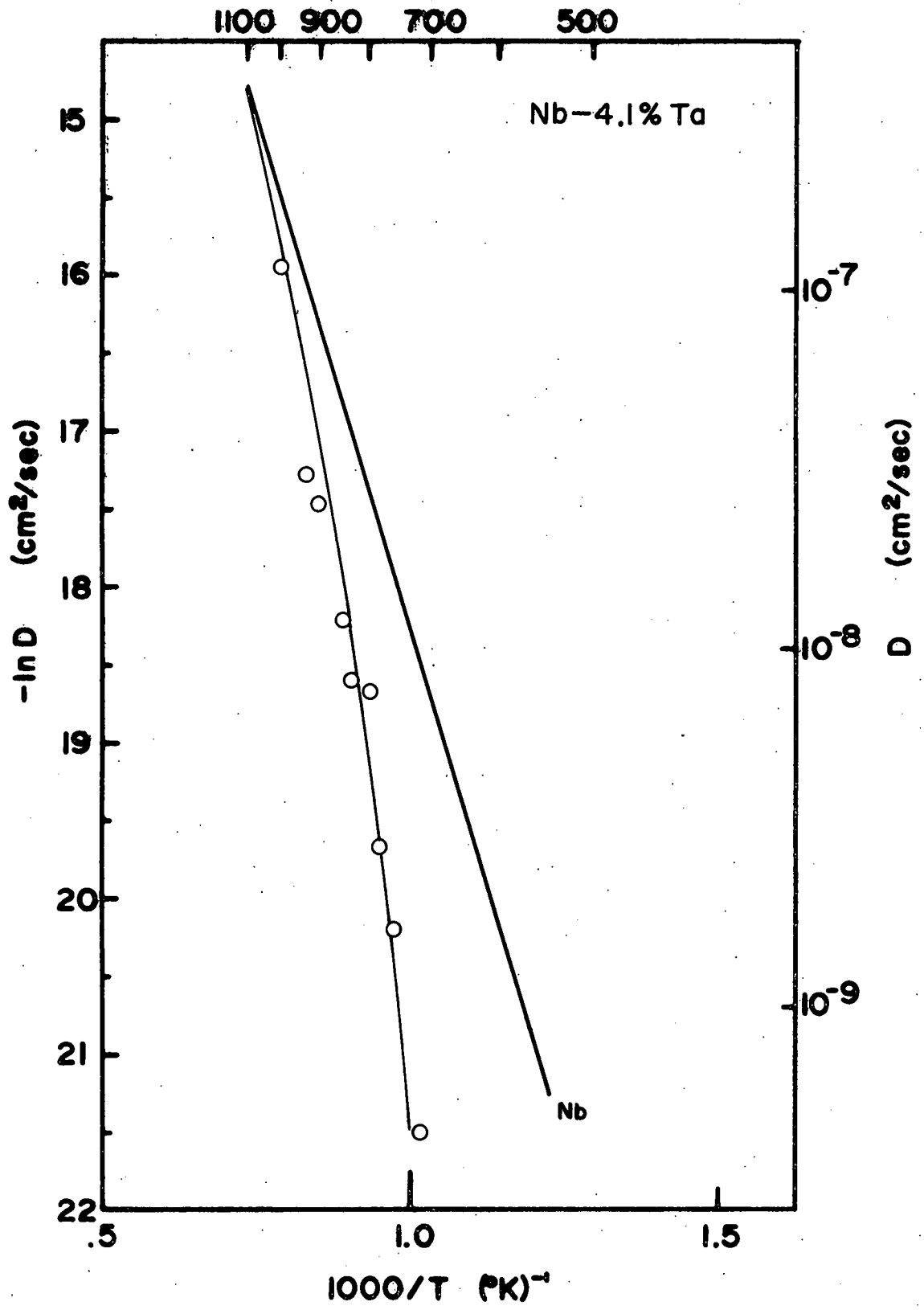

Figure 27: Arrhenius plot for the diffusion of oxygen in the Nb-4.1Ta alloy. The curve represents diffusivity predicted by the Oriani model, modified for variable trap energy.

like the others, but allowing a larger uncertainty in the trap energy.

2. Perkins and Padgett: In general, this model was not as satisfactory as the Oriani model for the alloys studied. For each alloy, a plot was made of $\ln\left[\frac{D_n}{D} - 1\right]$ versus $1/T$. The slope is then equal to H_b/k_B and the intercept at $1/T=0$ is equal to S_b/k_B. However, when presented in this form, the scatter becomes much more severe. The slope of this line can be calculated by a linear regression, but the correlation coefficient (fit) is not good. Also, from the temperature range of this study, it is a dangerously large extrapolation to $1/T=0$ to obtain the binding entropy.

The results of this model are summarized below and compared to those of the Oriani model:

TABLE VI

Comparison of Perkins and Padgett Model and Oriani Model

Alloy	"H_b" (eV) Perkins	"E_x" (eV) Oriani
Nb-1.4V	-0.51	-0.55
Nb-2.7V	-0.51	-0.53
Nb-5.1V	-0.56	-0.55
Nb-0.9Ti	-0.53	-0.7
Nb-0.95Zr	-0.55	-0.7

The failure of the Perkins and Padgett model to provide a consistent value for the O-V binding enthalpy raises serious doubts about its suitability for these systems (or at least for these data.) It is, unfortunately, very sensitive to errors in the lowest-temperature data points, and it is just these points that are often the least reliable. If data were available of the same accuracy as those for the pure metals, this model would no doubt be acceptable for calculating H_b. Still, calculations of S_b would not be very reliable unless the temperature range were extended somewhat.

3. Finite-Difference Method: The results (59) obtained by the finite-difference method (51) for the Nb-0.95Zr alloy are summarized in Table V and compared to the results of the Oriani model. It can be seen that in terms of the trap energy, the agreement is not good. When a plot was made of the logarithm of the equilibrium constant (as calculated from k/p) versus 1/T the result was definitely not a straight line. Thus, a least-squares analysis to obtain the trap energy by equation (8) is probably not valid. Of course, the connection between the equilibrium constant and the ratio of the trapping and release coefficients may be less direct than was previously thought. To settle this question definitively, one would need to know more about the actual structure of the trap, i.e., the height of energy barriers and the depth of energy wells close to the substitutional atom.

4. Summary: For the substitutional solutes considered in this study (with the possible exception of tantalum) the Oriani

model appears to be the most useful. The simplifications that distinguish it from the models of McNabb and Foster (48) and Koiwa (50) appear to be valid for the present alloys and temperature range. Following the Oriani approach, a change in the trap energy of 0.05 eV produces a measurably large change in the predicted diffusivity. Taking 0.05 eV as the minimum uncertainty, it is encouraging to note that the O-V trap energies calculated from the three Nb-V alloys (1.4 to 5.1%V) were all in agreement. On the other hand, elements with greater trap energies were readily distinguished from vanadium. Thus, the difference between elements was large relative to their individual uncertainties.

The data obtained in this study have provided a critical test of these models. The Oriani model proved most suitable by distinguishing four different trapping elements, and at the same time "recognizing" one element in three different concentrations.

4.2.4 Comparison with Other Reported Data

The diffusion data for pure niobium and pure vanadium are in excellent agreement with the results of previous work (29,30). For niobium, a summary of the previous data (29) indicated that Q^{Nb}=26100 cal/mole (109 kJ/mole). With the data from this work included, the result is Q^{Nb}=26400 cal/mole (110 kJ/mole), or a change of 0.8%. Perkins and Padgett (34) report a somewhat lower value of Q^{Nb}=25900 cal/mole (108 kJ/mole). But, the present results confirm their findings that the diffusivity of oxygen is independent of its concentration.

For vanadium, previous work indicated (30) a value of Q^V=29800 cal/mole (125 kJ/mole). The addition of the present data results in the following value: Q^V=29400 cal/mole (123 kJ/mole) or a change of 1.4%.

There is a wealth of literature on s-i interactions in various systems. The overall quality and accuracy are highly variable, and there are few data on the alloy systems investigated in this study. To provide an overview of the situation, Table VII lists some reported values for s-i binding energies in various systems.

TABLE VII

Substitutional-Interstitial Binding Energies

Matrix	s-i Pair	Binding energy eV	Binding energy kJ/mole	Reference
Nb	Zr-O i	>1.0	>96	33
	Zr-N i	0.31	30	36
	Zr-O d	0	0	34
	Zr-O d	0.7	67	Present work
	Ti-O d	0.7	67	"
	V-O d	0.55	53	"
	Ta-O d	0.3	29	"
Ta	Re-N i	0.14	14	35
	Re-O i	>0.14	>14	35
V	Ti-O i	0.26 ±0.4	25 ±39	41
	Al-O i	0.14	14	41
	Be-O i	0.27	26	41
Fe	Ti-N i	1.3	125	61
	V-O d *	0.29	28	37
	V-N d *	0.25	25	37
	Nb-N d *	0.21	20	37

i = internal friction
d = long-range diffusion

*liquid solutions

There have been several attempts in the past to develop a model that can relate the s-i binding energy to some easily determined properties of the substitutional element (39-41). The major obstacle in most cases is a lack of good data for a sufficient number of substitutional elements. A second obstacle seems to be the inclusion of so many parameters that the model becomes unworkable. Szkopiak and Smith (40) in particular have tried to tie in so many parameters that some simple relationships among the data are overlooked.

An added difficulty is the use of internal friction data to estimate s-i binding energies. When a distinct s-i peak is observed, interpretation is straightforward. However, there is some disagreement in the literature concerning the interpretation of data when there is only a broadening of the primary Snoek peak (41). A model cannot be based on data which some workers interpret as attractive s-i interaction and others interpret as s-i repulsion. The data in the present study demand a less equivocal interpretation.

Before developing a model to explain the results of the present study, it is necessary to understand the significance and limitations of the parameter ΔE_x. According to a strict application of the Oriani model, it is the energy difference between a normal interstitial site and each of the six "extra-ordinary" sites surrounding the substitutional solute atom. The assumption is that NNN sites (cube edges) are normal sites. This is probably not quite true. A recent study (52) indicated the importance of O-O interactions between NNN and possibly up

to third-NN oxygen atoms. Thus, it is not unreasonable to expect some interaction between the substitutional atom and NNN oxygen atoms. The effect of including more sites as traps is not large. (Adding all of the NNN sites would result in a decrease in the trap depth of only about 20%.) The important thing to note is that these geometric considerations affect all of the solutes equally, and thus do not interfere with the development of a predictive model based exclusively on data obtained by this EMF-method. However, caution must be used when trying to compare the present results to those obtained by anelastic techniques.

With this qualification understood, it is now possible to enumerate the principles on which the present model is based.

1. Chemical affinity: If the substitutional solute has a higher affinity for oxygen than the host element, there will be a s-i attraction which will be roughly proportional to the difference in oxygen affinities. A quantitative measure of oxygen affinity per se is not generally available, but a good approximation is probably given by the heat of formation of the oxide, expressed in eV/oxygen atom.

2. Elastic interaction: The interaction between the strain fields of the interstitial and substitutional solute atoms could result in an attractive or repulsive s-i interaction, depending on whether the substitutional atom is smaller or larger than the host atom.

3. Other effects: Parameters such as atomic compressibility,

atomic polarizability, or local changes in the elastic modulus of the host lattice are ignored. This keeps the model simple enough that possible non-linearities in the two major modes of interaction could be determined, given data for a large enough number of alloys.

The data for the four alloy systems examined in this study are presented below, along with the chemical affinity and size mismatch terms for each. (Also included are the values of these parameters for hafnium, and its "predicted" trap energy.)

TABLE VIII

Parameters Affecting Substitutional-Oxygen Interactions in Niobium

Element	Observed Trap Energy ΔE_x (eV)	Chemical Affinity, A (eV)	Size Mismatch ϵ (%)
Ta	0.3	0.13	0
V	0.55	0.13	-7.7
Ti	0.7	0.52	0
Zr	0.7	1.39	+11.2
Hf	(0.8-1.0)*	1.68	+10.5

*Predicted

The proposed model may thus be expressed by the following general formula:

$$\Delta E_x = f(A) + g(\epsilon) \qquad (38)$$

where

$$A = \Delta H^f_{NbO} - \Delta H^f_{MO} \quad \text{eV/oxygen atom} \qquad (39)$$

and $$\epsilon = \frac{r_{Nb} - r_M}{r_{Nb}} \qquad (40)$$

where r_X is the atomic radius of the species X.

The present data are not extensive enough to determine analytical expressions for f(A) and $g(\epsilon)$, but from the results shown in Table VIII several observations can be made. It can be seen that Ta and V are chemically similar, yet V is a stronger trap, due to its smaller size. Zirconium, on the other hand, has a greater chemical affinity for oxygen than titanium does, but the elastic repulsion due to its larger size partly offsets the chemical attraction so that Zr and Ti have about the same trapping strength. It is interesting to note that Szkopiak and Smith (40) report that hafnium is a stronger trap than zirconium. On the basis of their complicated model, they cannot understand how this can be so. But, that observation is in agreement with the prediction of the present model.

One difficulty that arises in using heats of formation to estimate oxygen affinities is the large number of compounds that some elements form, e.g., VO, V_2O_3, VO_2, V_2O_5, etc. The heats of formation of these compounds (in eV/oxygen atom) are all different, and the prediction of the model will depend on which value is selected. If the value for the MO-type oxide is used, a problem is then encountered with elements such as tantalum, for which there is no stoichiometric compound corresponding to TaO. (Szkopiak and Smith (40) introduced a great deal of confusion by neglecting to divide by the number of oxygen atoms. Thus, they compare Ta_2O_5 = 504 kcal/mole and

NbO = 102 kcal/mole and cannot understand why tantalum isn't a vigorously trapping solute.)

Hasson and Arsenault (39) point out that the correlation between heats of formation of the substitutional-element oxides is not as straightforward in the Group V systems as it is in the iron-based ternary alloys. They suggest that this is due to the greater degree of clustering of O-O pairs in the Group V alloys.

One method of evaluating the elastic term is given by Hashizume and Sugeno (62). For the case of Si-N interaction in iron, the value for the elastic contribution is given as ΔE_e=0.21 eV. The following expressions were developed (62):

$$\Delta E_e = 2(C_{11}-C_{12})(E_1-E_2)e_{\theta\theta}C^3 \qquad (41)$$

where C_{11} and C_{12} are the elastic constants of the alloy and E_1 and E_2 are the principal values of the strain tensor that characterizes a nitrogen atom in a normal octahedral site, and C is the lattice parameter. Also,

$$e_{\theta\theta} = \frac{\frac{1}{3}(r_{Si}^3 - r_{Fe}^3)}{r_{Fe}^3} \qquad (42)$$

When typical values are used for the case of oxygen in niobium, the result is an elastic term of 2 to 3 eV. This term is attractive or repulsive, depending on whether the substitutional atom is smaller or larger than the Nb atom. The values calculated by this method seem high by about a factor of five. Blanter and Khachaturyan (63) calculate the interaction between a vacancy

and an oxygen in a NN position to be 0.4 eV. Since the vacancy can be thought of as the limiting case of a very small substitutional atom, it is unlikely that a real substitutional atom (e.g., vanadium) could interact elastically to produce several eV of elastic strain energy. At the same time, it is not clear that Blanter and Khachaturyan (63) are justified in using an elastic model, when they calculate NN atom displacements around the oxygen to be 20% of the lattice parameter.

While there is disagreement concerning the magnitudes of the elastic interactions, it seems clear that a smaller atom will attract an interstitial, while a larger one will repel the interstitial, ceteris paribus.

4.2.5 Microhardness Measurements

The microhardness data for all three selected alloys showed the following characteristics:

1. A substantial overall softening of the alloy after contact with the zirconium block at high temperatures.

2. A general downward trend in the hardness of the alloy going toward the interface.

3. A general downward trend in the hardness of the zirconium going away from the interface.

These three observations are consistent with the assumptions that the zirconium block is acting as a sink for oxygen and that the change in cell EMF with time is due to outward diffusion of oxygen rather than precipitation within the sample.

The scatter in the data points is, in general, due to the

fact that some of the samples are probably two-phase at room temperature. This was a problem particularly when the Knoop indenter was used. When the data were retaken with a 136° Diamond Pyramid indenter and a somewhat larger load, this source of error was decreased. The 136° indentor also reduced the scatter that was due to the anisotropy of the polycrystalline zirconium block.

The data for the Nb-Ti-O alloy, Figure 22, best show the various effects mentioned. The hardness in the as-doped condition is substantially higher than the hardness after diffusion has occurred. To the alloy, the interface is an oxygen sink. To the zirconium block, on the other hand, the interface is an oxygen source. The motion of the oxygen across the interface is a good example of the phenomenon of "uphill diffusion" first analyzed in detail by Darken (64).

The data for the Nb-V-O alloy show the same general trends, Figure 23, but the scatter is more severe. The hardness profile in the zirconium block is more well-behaved, because it is probably still a solid solution at the end of the EMF run.

The data for the V-O alloy, Figure 24, show a very great decrease in hardness due to the oxygen loss. The final hardness (~75 DPH) indicates that some oxygen is still present (65). The wide variation in the hardness of the zirconium block is due to the formation of an extremely hard, brittle phase which was seen to grow into the zirconium at an angle to the interface. This phase had a blocky or platelike morphology. A hardness

profile that progressed normal to the interface could first encounter this phase at some distance from the interface. This resulted in some abnormally high readings at locations of .010-.015 in. (.254-.381 mm) from the interface. This effect was not observed in the other two specimens, because the amount of oxygen transferred was not great enough to cause the large quantity of second phases.

It is interesting to note that the Nb-Ti-O alloy was doped to 1.0% oxygen, while the Nb-V-O alloy was doped to 0.6% O. These facts are in qualitative agreement with the observations that: a) the Nb-Ti-O alloy in the as-doped condition is harder than the corresponding Nb-V-O specimen, and b) there is slightly more hardening in the zirconium block due to outward diffusion of oxygen from the Nb-Ti-O alloy than from the Nb-V-O sample.

4.2.6 Auger Electron Spectroscopy

To compare the amplitudes of oxygen and niobium (as outlined in Section 3.2.4) the 510 eV oxygen and 197 eV niobium peaks were used. In the vanadium, interference from the 509 eV vanadium peak made it necessary to use the weaker 490 eV oxygen peak and the 437 eV vanadium peak.

The information obtained by the use of AES provides clear evidence that the zirconium is a very efficient sink for oxygen. It confirms the validity of the assumption that the mode of oxygen removal is by outward diffusion rather than internal precipitation. The striking agreement between EMF data, microhardness data, and AES data can be seen in Table IX.

TABLE IX

Comparison of Analytical Data

Alloy	$\frac{C^*_{surface}}{C_o}$	$\frac{DPH^{ave}_{final}}{DPH_{initial}}$	$\frac{AR_{final}}{AR_{initial}}$
Nb-2.7V	0.5	0.82	0.72
Nb-0.9Ti	0.5	0.62	0.45
V	0.09	0.12	0.13

*Estimated from EMF data.

The good agreement between the microhardness technique and the AES technique indicates that both of these analytical tools are suitable for use with these alloys.

Using the Auger microprobe in the absorbed-current imaging mode, it was possible to photograph the second-phase regions in the zirconium block adjacent to the V-O alloy. These appear in Figure 25(a) as light areas close to the interface.

5. CONCLUSIONS

1. Oxygen obeys Henry's Law in niobium-tantalum alloys up to the solubility limit of the first oxide phase. The standard entropy and enthalpy of solution of oxygen in these alloys are intermediate between those of oxygen in pure niobium and pure tantalum.
2. The oxygen partial pressure in equilibrium with a Nb-Ta solid solution containing oxygen can be expressed as follows:

$$P_{O_2} = X_O^2 \exp \frac{2}{R}\left[\frac{-389000+45.5X_{Nb}}{T} + 60.9-0.055X_{Nb}\right]$$

   where R is in joules/mole-^oK, X's are in atomic %, and P_{O_2} is in atmospheres.
3. The EMF-method is suitable for studying the transient diffusion of oxygen in vanadium, niobium, and niobium alloys.
4. The diffusion of oxygen in several dilute substitutional niobium alloys is slower than it is in pure niobium. This appears to be due to the trapping of oxygen atoms by the substitutional solute atoms.
5. The effect of substitutional-interstitial interactions on the interstitial diffusivity can be approximately explained by theoretical models that take into account the concentration of substitutional atoms and the binding or "trap" energy associated with neighboring interstitial sites.
6. The substitutional solutes examined in this study are, in order of increasing trapping strength: tantalum, vanadium,

titanium, and zirconium.

7. The trap energy does not appear to depend on the substitutional concentration, up to about 5%. It is also not a function of oxygen concentration.
8. The substitutional-interstitial binding energy appears to be the sum of a chemical affinity term and an elastic term. For all of the alloy systems studied, the net chemical affinity was attractive. The elastic, or "misfit" energy was attractive, neutral, or repulsive, depending on the size of the particular substitutional atom.

APPENDIX

The computer technique for analyzing diffusion with trapping may be summarized as follows (59).

The general equation for diffusion with trapping, as given by the Caskey and Pillinger (51) treatment of the McNabb-Foster model (48) is:

$$\frac{\delta C}{\delta t}+N\frac{\delta n}{\delta t}=D\,\nabla^2 C$$

where C = concentration of diffusing species

N = traps per cm^3

n = fraction of traps occupied

and $$N\frac{\delta n}{\delta t}=NkC(1-n)-pnN$$ (conservation of solute atoms)

or, $$\frac{\delta n}{\delta t}=kC(1-n)-pn$$

where k and p are rate constants for trapping and release, respectively, of diffusing solute at fixed trapping sites.

To simplify computation, the equations are written in dimensionless form:

$$\frac{\delta U}{\delta \tau}+\frac{\delta W}{\delta \tau}=\nabla^2 U \qquad (1)$$

and $$\frac{\delta W}{\delta \tau}=\lambda U-\mu W-\nu UW \qquad (2)$$

where $U=C/C_o$ relative concentration of diffusing solute

$W=nN/C_o$ relative concentration of trapped solute atoms

$\tau=Dt/L^2$ reduced time

$X=x/L$ relative distance

$\lambda=NkL^2/D$

$\mu=pL^2/D$

$\nu=C_okL^2/D$

In these expressions, C_o is some reference concentration, such as the initial or surface concentration, and L is a reference distance, such as the thickness of the specimen.

At equilibrium,

$$\frac{\delta n}{\delta \tau}=kC(1-n)-pn=0$$

Thus, $$n=\frac{kc}{p+kc}$$

Initially, $$n_o=\frac{kC_o}{p+kC_o}$$

To find the finite-difference solution, the thickness of the plate is divided into M intervals. Define $U_o^o \ldots\ldots U_M^o$ and $W_o^o \ldots\ldots W_M^o$ initially, and change the values at successive times: $U_o^n \ldots\ldots U_M^n$, $W_o^n \ldots\ldots W_M^n$. This is done in the following manner.

Expand a Taylor's Series in time:

$$U_m^{n+1} = U_m^n + \frac{\delta U}{\delta \tau}\Big|_m^n \Delta\tau + \ldots\ldots \text{(small h.o.t.)}$$

This is done for both U and W.

Expand a Taylor's Series in space, and include the second order term:

$$U_{m+1}^n = U_m^n + \frac{\delta U}{\delta X}\Big|_m^n \Delta X + \frac{1}{2}\frac{\delta^2 U}{\delta X^2}\Big|_m^n (\Delta X)^2 = \ldots\ldots(\text{h.o.t.})$$

Solving, $$\frac{\delta U}{\delta \tau}\simeq\frac{U_m^{n+1}-U_m^n}{\Delta\tau} \qquad \text{etc.}$$

Substituting these into equation (2):

$$\frac{U_m^{n+1}-U_m^n}{\Delta\tau}+\frac{W_m^{n+1}-W_m^n}{\Delta\tau}=\frac{(U_{m+1}^n-2U_m^n+U_{m-1}^n)}{(\Delta X)^2}$$

A long-standing rule for solving such equations by the finite-difference technique specified a relation between the size of the time interval and the size of the space interval:

$$\frac{\Delta\tau}{(\Delta X)^2}<\tfrac{1}{2}$$

Generally, if this rule was not obeyed, the resulting solution would diverge. A contribution of Caskey and Pillinger (51) was to note that if some contribution from the future time interval is mixed with the present value, the solution will converge, even for larger values of $\Delta\tau/(\Delta X)^2$. This facilitates computation, since the time intervals can be made larger.

The final result is:

$$\frac{U_m^{n+1}-U_m^n}{\Delta\tau}+\frac{W_m^{n+1}-W_m^n}{\Delta\tau}=\left[\frac{\theta}{(\Delta X)^2}\cdot(U_{m+1}^{n+1}-2U_m^{n+1}+U_{m-1}^{n+1})+\frac{(1-\theta)}{(\Delta X)^2}\cdot(U_{m+1}^n-2U_m^n+U_{m-1}^n)\right]$$

where $\theta=0.5$ commonly.

Also,

$$\frac{W_m^{n+1}-W_m^n}{\Delta\tau}=\left[\theta(\lambda U_m^{n+1}-\mu W_m^{n+1}-\nu U_m^{n+1}W_m^{n+1})+(1-\theta)(\lambda U_m^n-\mu W_m^n-\nu U_m^n W_m^n)\right]$$

Thus, θ is the parameter that governs the mixing of past and

future times.

After expansion and rearrangement, the following expressions are obtained.

$$-A_m p_{m+1} + B_m p_m - C_m p_{m-1} = D_m \qquad (3)$$

and $$q_m = R_m p_m + S_m$$

where $$R_m = \frac{\theta(\lambda - \nu W_m^n)}{\theta(\mu + \nu U_m^n) + (1/\Delta\tau)}$$

$$S_m = \frac{\lambda U_m^n - \mu W_m^n - \nu U_m^n W_m^n}{\theta(\mu + \nu U_m^n) + (1/\Delta\tau)}$$

$$A_m = \theta$$

$$B_m = \frac{(\Delta X)^2}{\Delta\tau}\left[1 + R_m\right] + 2\theta$$

$$C_m = \theta$$

$$D_m = U_{m+1}^n - 2U_m^n + U_{m-1}^n - S_m \frac{(\Delta X)^2}{\Delta\tau}$$

These equations need only be solved for p_m. Caskey and Pillinger obtained solutions to equation (3) such that:

$$E_m = \frac{A_m}{B_m - C_m E_{m-1}} \qquad m > 1$$

and $$F_m = \frac{D_m + C_m F_{m-1}}{B_m - C_m E_{m-1}} \qquad m > 1$$

Then $U_m^{n+1} = p_m + U_m^n$ and $W_m^{n+1} = q_m + W_m^n$.

The fact that E_m and F_m are equal to zero at the surface provides the initial values. At successive times, U and W are adjusted using the expressions above.

The computer program written by Robert Frank (59) calculates the concentration as a function of time for the appropriate boundary conditions. The values of C(t) are then converted to EMF(t) and plotted, along with EMF(t) for simple diffusion (no trapping). The ratio of the trapping and release coefficients, k/p, is then adjusted until the slope of the calculated EMF(t) curve matches the slope of an experimentally determined curve. From the k/p values, the equilibrium constants and "trap energy" can be calculated and compared to the results of other models.

LIST OF REFERENCES

1. K. Kiukkola and C. Wagner, J. Electrochem. Soc. 104, 379 (1957).
2. K. Kiukkola and C. Wagner, J. Electrochem. Soc. 104, 308 (1957).
3. T. Etsell and S. Flengas, Chem. Rev. 70, 339 (1970).
4. J. Patterson, E. Bogren, and R. Rapp, J. Electrochem. Soc. 114, 752 (1967).
5. A. Rao and V. Tare, Scripta Met. 5, 813 (1971).
6. R. Rapp, Thermodynamics of Nuclear Materials, IAEC, Vienna, p. 75 (1967).
7. C. Alcock and B. Steele, Science of Ceramics, The British Ceramic Society, vol. II, 397 (1965).
8. B. Steele and C. Alcock, Trans. Met. Soc. AIME 233, 1359 (1965).
9. E. Fromm, J. Less-Common Metals 14, 113 (1968).
10. E. Fromm and H. Jehn, Met. Trans. 3, 1685 (1972).
11. R. Elliot, Trans. ASM 52, 990 (1960).
12. R. Bryant, J. Less-Common Metals 4, 62 (1962).
13. A. Taylor and N. Doyle, J. Less-Common Metals 13, 313 (1967).
14. E. Gebhardt and R. Rothenbacher, Z. Metallk. 54, 623 (1963).
15. A. Seyboldt, Trans. AIME 200, 774 (1954).
16. P. Kofstad, J. Less-Common Metals 7, 241 (1964).
17. M. Andrews, J. Amer. Chem. Soc. 54, 1845 (1932).
18. H. Jehn and E. Olzi, J. Less-Common Metals 27, 297 (1972).
19. E. Gebhardt and H. Preisendanz, Z. Metallk. 46, 560 (1955).
20. D. Vaughn, O. Stewart, and C. Schwartz, Trans. AIME 221, 937 (1961).
21. E. Gebhardt and H. Seghezzi, Z. Metallk. 48, 503 (1957).

22. M. Parkman, R. Pape, R. McRae, D. Brayton, and L. Reed, NASA Contractor Report CR-1276.

23. E. Gebhardt and H. Seghezzi, Z. Metallk. 50, 521 (1959).

24. H. Koberle, Dissertation, Tech. Hochschule, Stuttgart, W. Germany (1959).

25. R. Kirchheim, Dissertation, Tech. Hochschule, Stuttgart, W. Germany (1971).

26. W. Nickerson and C. Altstetter, Scripta Met. 7, 229 (1973).

27. W. Nickerson and C. Altstetter, Scripta Met. 7, 377 (1973).

28. E. Rudy, Compendium of Phase Diagram Data, Part V, Air Force Materials Laboratory Report AFML-TR-65-2 (1969).

29. F. Boratto and R. Reed-Hill, Met. Trans. 8A, 1233 (1977).

30. F. Boratto and R. Reed-Hill, Scripta Met. 11, 1107 (1977).

31. P.Bunn, D. Cummings,and H. Leavenworth, J. Appl. Phys. 33, 3009 (1962).

32. R. Miner, D. Gibbons, and R. Gibala, Acta Met. 18, 419 (1970).

33. C. Wert, J. Phys. Chem. Solids 31, 1771 (1970).

34. R. Perkins and R. Padgett, Acta Met. 25, 1221 (1977).

35. A. Sagues and R. Gibala, Acta Met. 22, 1423 (1974).

36. D. Mosher, C. Dollins, and C. Wert, Acta Met. 18, 797 (1970).

37. R. McLellan and R. Farraro, Acta Met. 25, 1217 (1977).

38. M. Mondino and A. Seeger, Scripta Met. 11, 817 (1977).

39. D. Hasson and R. Arsenault, Treatise on Materials Science, Vol. 1, Academic Press, New York (1972).

40. Z. Szkopiak and J. Smith, J. Phys. D, Appl. Phys. 8, 1273 (1975).

41. T. Shikama, S. Ishino, and Y. Mishima, J. Nucl. Mat. 68, 315 (1977).

42. L. Dijkstra and R. Sladek, Trans AIME 197, 69 (1953).

43. J. Enrietto, Trans AIME 224, 47 (1962).

44. J. Snoek, Physica 6, 711 (1941).

45. R. McLellan, M. Rudee, and T. Ishibashi, Trans. AIME 233, 1938 (1965).

46. R. Condit and D. Beshers, Trans. AIME 239, 680 (1967).

47. D. Beshers, Diffusion of Interstitial Impurities, in Diffusion, ASM, Metals Park, Ohio (1973).

48. A. McNabb and P.Foster, Trans AIME 227, 618 (1963).

49. R. Oriani, Acta Met. 18, 147 (1970).

50. M. Koiwa, Acta Met. 22, 1259 (1974).

51. G. Caskey and W. Pillinger, Met. Trans. 6A, 467 (1975).

52. G. Steckel, PhD Thesis, University of Illinois (1978).

53. D. Potter, PhD Thesis, University of Illinois (1970).

54. G. Steckel and C. Altstetter, Acta Met. 24, 1131 (1976).

55. R. Kirchheim, E. Albert, and E. Fromm, Scripta Met. 11, 651 (1977).

56. J. Crank, The Mathematics of Diffusion, Oxford University Press, London, p. 58 (1957).

57. F. Schmidt and J. Warner, J. Less-Common Metals 13, 493 (1967).

58. E. Gebhardt and R. Rothenbacher, Z. Metallk. 54, 443 (1963).

59. R. Frank, personal communication.

60. R. Predmore and R. Arsenault, in Proc. Int'l. Conf. on Mechanical Behavior of Materials, Kyoto, Japan, p. 155 (1971).

61. G. Szabo-Miszenti, Acta Met. 18, 477 (1970).

62. H. Hashizume and T. Sugeno, Jap. J. Appl. Phys. 6, 367 (1967).

63. M. Blanter and A. Khachaturyan, Met. Trans. 9A, 753 (1978).

64. L. Darken, Trans. AIME 180, 430 (1949).

65. O. Carlson, F. Schmidt, and D. Alexander, Met. Trans. 3, 1249 (1972).

VITA

The author was [redacted]. He graduated from Lane Technical High School in June, 1969. In September of the same year, he entered the University of Illinois. In May, 1974, he received the degree of Bachelor of Science with High Honors in Civil Engineering (Structures.) In August, 1974, he received the degree of Master of Science in Metallurgical Engineering. After one year as a Development Engineer at Caterpillar Tractor Company, he returned to the Graduate College of the University of Illinois.

He is a member of the American Society for Metals and a member of Chi Epsilon National Honorary Civil Engineering Fraternity. He has co-authored one publication, entitled "Thermodynamic Properties of Niobium-Tantalum-Oxygen Solid Solutions," by R. J. Lauf and C. J. Altstetter, Scripta Met. 11, 983 (1977).